THE GEDIZ RIVER FLUVIAL ARCHIVE:
A BENCHMARK FOR QUATERNARY RESEARCH IN WESTERN ANATOLIA

Maddy, D.[1*], Veldkamp, A.[2], Demir, T.[3], van Gorp, W. [4], Wijbrans, J.R. [5], van Hinsbergen, D.J.J[6]., Dekkers, M.J. [6], Schreve, D.[7],Schoorl, J.M. [8], Scaife, R. [9], Stemerdink, C.[1], van der Schriek, T.[1], Bridgland, D. R. [10] and Aytaç, A.S. [11]

1. School of Geography, Politics and Sociology, Newcastle University, Newcastle upon Tyne, NE1 7RU, UK
2. Faculty of Geo-Information Science and Earth Observation (ITC), Twente University, Enschede, The Netherlands
3. Akdeniz Üniversitesi, Edebiyat Fakültesi, Coğrafya Bölümü, Konyaaltı-Antalya, Turkey.
4. Groningen Institute of Archaeology (GIA), University of Groningen, Poststraat 6, 9712 ER , Groningen, The Netherlands
5. Department of Earth Science, VU University, De Boelelaan 1085, 1081 HV Amsterdam, The Netherlands
6. Department of Earth Sciences, Utrecht University, Heidelberglaan 2, 3584 CS Utrecht, the Netherlands
7. Department of Geography, Royal Holloway University of London, Egham, TW20 0EX, UK
8. Soil Geography and Landscape group, Wageningen University, P.O. Box 47 6700AA, Wageningen, The Netherlands.
9. School of Geography and Environment, University of Southampton, Southampton SO17 1BJ, UK
10. Department of Geography, Durham University, South Road, Durham DH1 3LE, UK
11. Department of Geography, Harran University, 63300 Sanliurfa, Turkey

ABSTRACT

The Gediz River, one of the principal rivers of Western Anatolia, has an extensive Pleistocene fluvial archive that potentially offers a unique window into fluvial system behaviour on the western margins of Asia during the Quaternary. In this paper we review our work on the Quaternary Gediz River Project (2001-2010) and present new data which leads to a revised stratigraphical model for the Early Pleistocene development of this fluvial system.

In previous work we confirmed the preservation of eleven buried Early Pleistocene fluvial terraces of the Gediz River (designated GT11, the oldest and highest, to GT1, the youngest and lowest) which lie beneath the basalt-covered plateaux of the Kula Volcanic Province. Deciphering the information locked in this fluvial archive requires the construction of a robust geochronology. Fortunately, the Gediz archive provides ample opportunity for age-constraint based upon age estimates derived from basaltic lava flows that repeatedly entered the palaeo-Gediz valley floors. In this paper we present, for the first time, our complete dataset of $^{40}Ar/^{39}Ar$ age estimates and associated palaeomagnetic measurements. These data, which can be directly related to the underlying fluvial deposits, provide age constraints critical to our understanding of this sequence.

The new chronology establishes the onset of Quaternary volcanism at ~1320ka (MIS42). This volcanism, which is associated with GT6, confirms a pre-MIS42 age for terraces GT11-GT7. Evidence from the colluvial sequences directly overlying these early terraces suggests that they formed in response to hydrological and sediment budget changes forced by climate-driven vegetation change. The cyclic formation of terraces and their timing suggests they represent the obliquity-driven climate changes of the Early Pleistocene. By way of contrast the GT5-GT1 terrace sequence, constrained by a lava flow with an age estimate of ~1247ka, span the time-interval MIS42 – MIS38 and therefore do not match the frequency of climate change as previously suggested. The onset of volcanism breaks the simple linkage of terracing to climate-driven change. These younger terraces more likely reflect a localized terracing process triggered by base level changes forced by volcanic eruption and associated reactivation of pre-existing faults, lava dam construction, landsliding and subsequent lava-dammed lake drainage.

Establishing a firm stratigraphy and geochronology for the Early Pleistocene archive provides a secure framework for future exploitation of this part of the archive and sets the standard as we begin our work on the Middle-Late Pleistocene sequence. We believe this work forms a benchmark study for detailed Quaternary research in Turkey.

1. INTRODUCTION

Over the past 150 years, fluvial archives have provided critical stratigraphical information key to the unravelling of continental stratigraphy, especially in Western Europe. The highly detailed but still incomplete database of Quaternary stratigraphical evidence generated in countries with long traditions of geological mapping has recently led to a shift away from the fundamental questions of stratigraphy towards a more focussed thematic approach targeted at, for example, hazard management and wealth creation. However, for large parts of the globe, where geological investigation is often in its infancy, there is still much basic mapping to be undertaken before a comparatively firm local-regional stratigraphy can be established.

At the outset, FLAG was initiated to promote work on fluvial archives worldwide by enhancing dialogue between workers from all continents. Fluvial archives from Europe and North America were well-represented, albeit still with gaps, in the literature, but little detailed work was available from elsewhere. It was clear, however, that some work had been undertaken in these areas of perceived data vacuum but considerable additional effort would be needed to make this work available to a wider audience. A further goal of FLAG was to begin harmonising the collection and reporting of observations, thus facilitating more effective regional comparisons

One such collaborative research programme to emerge from the early meetings of FLAG was an attempt to move just beyond the boundaries of Europe into western Asia by looking at the fluvial archives of Anatolia (Turkey). Specifically, as a result of a chance meeting with Dr Rob Westaway and his Turkish collaborator, Dr Sema Yurtmen, we were introduced to exposures of fluvial sediments attributed to deposition by an ancestral Gediz River and its tributaries in the region of the Kula Volcanic Province. The Gediz River, at ~275km in length, is one of the principal rivers of Western Turkey (Figure 1) and thus a prime target of interest. Although this area has been mapped by the MTA (Mineral Research & Exploration General Directorate. Ercan *et al.*, 1983), these fluvial deposits are largely buried beneath basaltic lava flows and thus surface maps do not display their geometry or extent. Indeed, the extensive surface exposures of dissected Miocene sediments dominate the maps with

very limited surface outcrop of superficial unconsolidated sediments of presumed Quaternary age often attributed to a poorly defined Asartepe Formation (Figures 2, 3). Given the extensive and often spectacular exposure of the Miocene Basin fill, it is not surprising that the thinner and buried Gediz River fluvial archive had been largely overlooked. Early results from our investigations were discussed during an excursion to the field area associated with the FLAG 2006 meeting based in İzmir.

The Gediz River Project (2001-2010) results reported here present our latest stratigraphical model for the Early Pleistocene development of this fluvial system. This outcome builds upon our previously reported work but, with the benefit of many new age estimates derived from associated lava flows and new observations, adds significantly to our understanding, with implications not only for stratigraphy but also for establishing fluvial-system drivers, environmental reconstruction and early hominin dispersal. We believe this work forms a benchmark study, signposting a way forward for detailed Quaternary research in Turkey.

2. Pre-Quaternary Stratigraphy and neotectonics in the Selendi Basin.

On its route to the Aegean Sea, the Gediz River traverses some of the most important tectonic structures of western Anatolia (Figure 2) including the NNE-SSW aligned Neogene Uşak-Güre, Selendi and Demirci Basins before entering the more recent, east-west orientated, Plio-Pleistocene Alaşehir (Gediz) Graben. Our principal area of interest, within the Kula Volcanic Province, is situated in the southern half of the Neogene Selendi Basin (Figures 2, 3), where the evolution of the Gediz river system reflects progressive incision into thick Miocene Basin fill sediments. Understanding the lithostratigraphy of the Basin fill and its principal structures is therefore an essential context for understanding the Quaternary river behaviour and the resulting fluvial archive.

The lithostratigraphy of the Selendi Basin fill was first described in detail by Ercan *et al*. (1983) but was subsequently revised by, amongst others, Seyitoğlu (1997), Purvis and Robertson (2004) and most recently by Ersoy *et al*. (2010). Table 1 shows the Cenozoic

stratigraphy based upon Ersoy *et al*. (2010), with the addition of the Gediz Valley Formation (see Maddy *et al*., 2012a).

The largely unconsolidated nature of much of the Basin fill provides a readily erodible, but spatially variable, substrate for vertical and lateral fluvial erosion/deposition and accompanying slope processes. The nature of this substrate thus varies through time as progressive fluvial incision proceeds, constraining valley geometry and therefore preservation potential, as lithological properties either promote or dampen opportunities for valley widening. Progressive incision into the Basin stratigraphy also leads to changing hydrology, especially where incision removes capping limestones and karstic drainage systems are abandoned. Faulting structures contribute to the spatial and temporal variability in the lithology of the substrate, in addition to providing areas of weakness, readily exploited by the fluvial system and helping to position channel courses. The faults also act as conduits for water and are often associated with hot water springs and the deposition of travertine. Finally, with the exhumation of the more resistant basement strata, the pre-Basin fill topography exerts increasing control over drainage directions as stripping of the overlying sediment proceeds.

The oldest basement rocks (Figure 2, 3) underlying the basin fill are the pre-Neogene metamorphics of the Menderes Massif (predominantly gneiss, schist, quartzite and marble). These rocks outcrop only in the south-eastern quadrant of our study area (Figure 3) and they structurally underlie Cretaceous ophiolites and ophiolitic mélange rocks that outcrop more extensively within our study area especially north of İbrahimağa where ophiolitic hills reach over 550m a.m.s.l. (Figure 3). Although these outcrops would have been buried beneath Basin fill for much of the earliest Quaternary, the exhumation of the hill tops, which lie within the altitudinal range of the Early Pleistocene Gediz valley floor (see below) is most likely to have occurred around ~1.5Ma. The significance of this change is discussed below.

The earliest deposits in-filling the Basin are the conglomerates and sandstones of the Hacıbekir Group (Kürtkőyü and Yenikőy Formations), which is generally accepted as Early Miocene in age (Seyitoğlu, 1997, Westaway *et al*., 2003, 2004). This Group has a restricted outcrop within the study area and comprises coarse grade and angular gravels interpreted

as alluvial fan facies derived from the topographic highs of the metamorphic and ophiolitic hills of the Early Miocene. These deposits, are extensively deformed, indicating an early Miocene phase of deformation (Purvis and Robertson, 2004). The current outcrops lie well beneath the levels of the Early Pleistocene Gediz river deposits and thus it is unlikely that these sediments were available to the river at that time. It remains possible, however, that sediments of the Hacıbekir Group may have been removed from the higher levels of the pre-Basin fill topography.

The İnay Group unconformably overlies the Hacıbekir Group. The stratigraphic sequence of the İnay Group records progressive in-fill of the Selendi Basin. Gently inclined to sub-horizontally bedded sands and silts up to ~200 m in thickness, (Ahmetler Formation, Balçıklıdere Member) are overlain by fine-grained sandstones and silts up to a few tens of metres in thickness (Ahmetler Formation, Gedikler Member). $^{40}Ar/^{39}Ar$ age estimates of 18.89 ± 0.58 Ma to 16.42 ± 0.09 Ma from intercalated tuff within the Gedikler Member in the Selendi Basin suggest an Early to early Middle Miocene age for these units (Purvis and Robertson, 2005). The İnay Group sequence is capped by up to ~300m of carbonaceous muds and silts, lacustrine facies of the Ulubey Formation, which represent the end stage of Basin fill. The age of the Ulubey Formation in the Selendi Basin can be no younger than the Late Miocene (see below). The sediments of the İnay Group are the predominant source of clastic sediments preserved with the Gediz Valley Formation.

The Basin fill sediments are subsequently deformed during the Late Miocene as a result of tectonic extension evidenced by the formation of large numbers of NNE-SSW trending normal faults (Yilmaz *et al*., 2000). The throws on these faults are reported by Bunbury *et al*. (2001) to be generally less than 100m based upon the offset of the Ulubey Formation. These offsets undoubtedly created significant topography across the former Miocene lake floor, which would have promoted drainage development. A number of these NNE-SSW trending faults cut across the study area and their exhumation often appears to guide contemporary river courses (Figure 4a).

Unconformably overlying the İnay Group is the Kocakuz Formation, comprising reddish conglomerates and minor sandstone, with locally laminated limestone lenses (Ersoy and Helvacı, 2007; Ersoy *et al*., 2010). This formation is capped on the eastern margin of the Selendi Basin by the Kabaklar basalt (Figure 2), which has $^{40}Ar/^{39}Ar$ age estimates of 8.37 ± 0.07 Ma (Innocenti *et al*., 2005), confirming a minimum Late Miocene age for the underlying Kocakuz Formation and by inference providing an upper age limit for the underlying İnay Group. The sediments ascribed to the Kocakuz Formation by Ersoy *et al*. (2010) had previously been mapped as Quaternary Asartepe Formation by Ercan *et al*.; (1983). This reassignment of former Asartepe Formation sediments may have implications for the study area where sediments mapped as Asartepe Formation crop out east and south of İbrahimağa (Figure 3). The Kocakuz Formation and the Kabaklar basalt are considered by Ersoy *et al*. (2010) to be genetically linked to a NW-SE-trending dextral oblique to strike slip fault, suggesting a phase of strike-slip deformation following the earlier extensional faulting but still within the Late Miocene.

A final phase of tectonic deformation is attributed to the Pliocene-Quaternary. This phase of north-south extension was responsible for the creation of the E-W striking high angle normal faults that bound the Alaşehir (Gediz) Graben to the south of the study area. Bozkurt (2001) suggests that this latest phase of extension began in the early Pliocene, ~5Ma, with acceleration of movement on the Alaşehir graben bounding faults during the Quaternary at ~1.6 Ma suggested from the biostratigraphy of uplifted sediments (Sarica, 2000). Significant E-W trending high-angle (>35°) normal faults attributed to the late Miocene- early Pliocene have been identified north of the study area in the central Selendi Basin, where they bound asymmetrical grabens up to ~10 km wide (Figure 2; Seyitoğlu *et al*., 1997, Purvis and Robertson, 2004). Purvis and Robertson (2004) report that these faults, which individually typically have <20 m offsets, cut all sedimentary units and therefore cannot be dated accurately. They also state, however, based upon the work of Seyitoğlu *et al.* (1997), Yilmaz *et al*., (2000, 2001) and Westaway (pers. comm. 2004), that these faults pre-date all Quaternary-age lava flows.

This final phase of faulting would, as in the case of the earlier Late Miocene faulting, have exerted further structural control over any evolving drainage pattern. The pattern of Pliocene drainage in the area is, however, unclear and connectivity between the drainage in the Selendi Basin and the Alaşehir graben uncertain. The sediments attributed to the Asartepe Formation in the study area by Ercan *et al*. (1983) may relate to this time interval. However, there is little observational data reported in the literature and their stratigraphical relationship to the Quaternary basalts is, at best, ambiguous. What is clear, however, is that the Late Miocene-Pliocene reorganisation of drainage is triggered by the deformation associated with regional tectonic extension. This deformation produces a regional gradient that ultimately forces water out of the Selendi Basin towards the evolving sink of the Alaşehir (Gediz) Graben. Differential crustal movements result in relative uplift in the study area, forcing the subsequent progressive incision into the basin fill. The forces that triggered incision are ongoing at present, ensuring continuing adjustment of the fluvial system. Dynamical adjustment of the Gediz River to uplift during the Quaternary is complicated, not only by the frequency of changing environmental conditions that control sediment and water availability, but also by localized disruptions to water and sediment supply caused by volcanism, lake formation and landsliding (Maddy *et al*., 2012b).

3. Quaternary Geology and the Gediz Valley Formation

The mapped Quaternary deposits of the study region are dominated by the basaltic lava flows of the Kula Volcanic Province. Prior to the Gediz River Project, a chronology of the Kula Volcanic Province was proposed based upon a small number of K-Ar age estimates and classification of flows into a relative sequence on the basis of topographic expression and the weathering characteristics of the observed lava flows (Erinç, 1970; Ercan, 1993. Ercan *et al*., 1983, 1996). The flows were categorized into four groupings ß1- ß 4 with ß1 the oldest and ß4 the youngest. Only lava flows relating to groups ß2-ß4 were identified in our study area. Basalts capping a number of high level plateaus e.g. the Burgaz, Sarnıç and İbrahimağa were attributed to the ß2 group (Figure 3). The youngest and freshest basalts were attributed to the ß4 group and all basalts at heights intermediate between the two, and more weathered than the youngest grouping, were attributed to the ß3 group (Figure 3). A

K-Ar age estimate of 1100ka (Borsi *et al*., 1972, no error margin given) from a ß2 flows (sampling location is uncertain) in the study area was Early Pleistocene in age, thus establishing a Quaternary assignment for all of the basalts of the study area.

Additional age estimates were reported for a number of flows by Richardson-Bunbury (1992) and these largely confirmed the existing subdivision suggesting that the flows in our field area represented three discrete phases of volcanic activity. Basalt samples taken in the early years of our Gediz River Project yielded further geochronological resolution (Westaway *et al*., 2004, 2006; *see* table 4) suggesting that these aforementioned phases of volcanic activity related to the Early, Middle and Late Pleistocene respectively. Geographically each phase was related to a zone of different eruption centres. Those furthest north, now on or around the basaltic plateaux were the oldest, with highly degraded volcanic cones or exposed volcanic necks. The volcanic centres for the Middle Pleistocene eruption centres lay further south and their flows occurred at lower altitudinal levels. Finally, the most recent eruption centres lay even further south and are situated closest to the Alaşehir (Gediz) graben and are evidenced by large cones and lava flows with relatively fresh, irregular surfaces. Some of these flows reach the current Gediz River north of Kula (Figure 3).

Although the work of Bunbury acknowledges an association of the lava flows north of Kula with underlying fluvial sediments (Bunbury *et al*., 2001), this work, which was largely based on a petrological and chemical study of the lavas (Richardson-Bunbury, 1992; 1996), failed to recognise the full complexity of the underlying sequence and thus arrives at conclusions which are readily refuted by the later Gediz Project observations. Similarly, only some of the age estimates presented by Westaway *et al*. (2004, 2006) relate to lava flows that have a clear, unequivocal, relationship to the underlying fluvial deposits, thus limiting their utility in establishing a secure chronology for the underlying fluvial sequence.

The early years of the Gediz River Project (2001-2004) identified previously unrecognised complexity within the buried Quaternary fluvial sedimentary sequence beneath the high level basaltic plateaux. Using detailed traditional survey measurements of critical contacts,

Maddy *et al*. (2005) identified eleven terraces of the Gediz River preserved beneath the basalt-covered Burgaz plateau, with each discrete Gediz terrace(GT) designated by a number from GT1 the lowest and youngest, to GT11 the highest and oldest (Figure 4a, Figure 5a-c). The terrace deposits lie above planar, near-horizontal, contacts with the underlying Ahmetler Formation (Figure 4b, Figure 5b). These bases have lateral extents up to ~200m wide but as these are truncated, the width of the former floodplains is unknown but likely to be less than 500m. The preservation of these terrace deposits is clearly the result of their fortuitous burial beneath the erosion-resistant capping lava flows (Figure 5c). Dissection of the area north of the Burgaz plateau eliminates any opportunity for the preservation of higher terrace units north of the lava-capped terraces. It is likely, however, that the formation and preservation of terraces was restricted to palaeo-valley floors developed on the readily erodible Ahmetler Formation. The less readily eroded calcareous beds of the Ulubey Formation currently allow only narrow and steep-sided valleys to form, a poor environment for terrace preservation. The highest terrace has a base below the Burgaz plateau at an altitude of ~615m a.m.s.l., which is within 30m of the Ahmetler Fm. / Ulubey Fm. contact exposed in the scarp to the north, thereby suggesting that the area between the Burgaz plateau and the current scarp (Figure 3) could have supported only a limited number of additional higher terraces prior to dissection. However, our observations suggest this area may have already been considerably deformed due to faulting (see below), making it highly likely that the GT11 terrace is the earliest possible preserved terrace of the palaeo-Gediz in this part of the Gediz catchment.

Using gradient projection of terrace bases, these outcrops were correlated with similar fluvial sediments downstream beneath the basalt-capped Sarnıç plateau (Figure 4a). Later mapping work (2005-2011) downstream of the original field area identified Gediz gravels beneath the basalt-capped İbrahimağa plateau (Figure 4a). These new data required a re-evaluation of the original assumed river gradient used for correlation of the terrace bases. The new higher gradients (~0.004 – 0.005) were consistent with the modern river gradient and as a result, a revised correlation model for the outcrops was proposed (Figure 6, after Maddy *et al*., 2012a). The recognition that the deposits of the palaeo-Gediz river could, on the basis of their lithological composition and sedimentary properties, be readily mapped

and distinguished from all other stratigraphical units led Maddy *et al*. (2012a) to propose that these distinctive sediments should be formally recognised as the Gediz Valley Formation. The numbering of individual terraces remains only an interim measure, each of these stratigraphical units will be replaced with appropriate Member names once work on the complete Gediz Valley Formation i.e. including our ongoing study of the Middle and Late Pleistocene fluvial units, is completed.

Detailed observations of the terrace sediments taken from >100 separate outcrops exposed along the dissected margins of the plateau, demonstrate clear stratigraphical relationships between the terraces and the earliest phase of volcanism within this part of the Kula Volcanic Province. The onset of local volcanism is signalled by a change in lithological content with the influx of substantive quantities of basalt into the river bedload post GT6 (Maddy *et al*., 2012a). This conclusion is further supported by the stratigraphy of key GT6 exposures beneath both the Burgaz and Sarnıç plateaux. Beneath the Sarnıç plateau, the sedimentology of GT6 deposits near Çakırca (Figure 3; see also figure 9A in Maddy *et al*., 2012a) strongly suggests deposition in standing water, a conclusion supported by the presence of thick lacustrine sediments that include substantive amounts of tephra in adjacent exposures. Similarly, beneath the Burgaz plateau, GT6 sediments are overlain by lacustrine sediments that onlap the older terraces (up to GT9), suggesting the formation of a large standing water body. The GT6 valley floor was thus blocked downstream, with a volcanic dam caused by lava incursion onto the valley floor being the most likely scenario.

Maddy *et al*. (2012a) suggest this initial volcanic dam was associated with the emplacement of lavas that cover the İbrahimağa plateau and they speculated that the most likely source was the Tavşan volcanic neck (no. 1, Figure 3). Lacustrine sediments deposited within the lake associated with this dam (Lake 1, Maddy *et al.*, 2012a) cover Gediz terrace sediments across much of the higher levels of the Burgaz and Sarnıç plateaux. Thick tephra beds intercalated with lacustrine sediment of the same lake on the eastern exposures of the Sarnıç plateau (Figure 5d) suggest a more local source from the Toytepe neck (no.3, Figure 3) and the presence of pillow structures in the lavas that cap Kavtepe suggest that this neck (no.5, Figure 3) may also have erupted directly into this lake. Thick (>50m) tephras close to

the Sarnıç Bağtepe volcanic neck (no.4, Figure 3) may also suggest eruption of that neck during this period. This stratigraphy suggests that the first eruptions came from volcanic centres situated either within or close to the İbrahimağa plateau with eruptions focused around the Burgaz and Sarnıç plateaux following shortly afterwards.

Establishing the age of the first eruption would provide a critical pinning point for the terrace sequence by providing a minimum age for the GT11-GT6 sequence and a maximum age for the GT5-GT1 sequence. Several attempts to obtain an $^{40}Ar/^{39}Ar$ age estimate from the Tavşan lava immediately adjacent to the neck have proved indeterminate. Westaway *et al*. (2006) report an age estimate of 1264± 15ka for a lava flow that caps the Çakırca sequence. This lava flow does not deform the underlying standing water sediments and thus appears to arrive after the lake (Lake 1) has drained. On this basis, Maddy *et al.,* (2012a) concluded that the earliest damming event must pre-date ~1264ka (MIS38, Lisieki and Raymo, 2005). By inference, Maddy *et al*. (2012a) thus also concluded that Gediz terraces GT11-6 must also pre-date this time.

The regular altitudinal separation between the bases of the higher terraces (GT11–GT6) suggested a cyclic control over their formation (Maddy *et al*., 2005). Terraces GT11-GT7 all have colluvial sediments overlying the fluvial deposits, which record post-abandonment environmental changes prior to their burial by either lacustrine or volcaniclastic deposits. These colluvial sequences contain numerous palaeosols that record cyclic changes alternating between wetter and dryer conditions, the latter frequently associated with calcrete formation (Maddy *et al.*, 2012b; Veldkamp *et al*., 2015). The thickness and complexity of these colluvial sequences is greatest on GT11 (up to ~5m thick), diminishing progressively in both thickness and stratigraphical complexity moving down the terrace sequence to GT7 where these deposits are <2m in thickness. Veldkamp *et al*. (2015) link the environmental changes recorded in these colluvial sequences to Early Pleistocene climate cycles and support the earlier suggestion of Maddy *et al*. (2005) of a direct link between cyclic climate change and terrace formation. Maddy *et al.* (2005) suggest that these cycles were most likely the obliquity-driven climate cycles recognised from Eastern Mediterranean ocean oxygen isotope records (Kroon *et al.*, 1998).

The lower terrace sequence (GT5-GT1) demonstrably post-dates GT6. In an attempt to put a minimum age on the terrace sequence, Maddy *et al*. (2012a) inferred that a lava flow that covers the eastern side of the İbrahimağa plateau, with the youngest available age estimate of ~999 ±21 ka (Westaway *et al.,* 2006), may, on the basis of its altitude, have entered the GT1 valley. However, there are currently no recorded exposures of sediments on the İbrahimağa plateau that can be securely correlated with GT1, thus the relationship of this flow to the terrace sequence is somewhat equivocal. Despite this complication, Maddy *et al*. (2012a) assigned GT1 to MIS28. This attribution led Maddy *et al*. (2012a) to the conclusion that terraces GT5-GT1 continued to reflect formation synchronous with climate change despite the obvious disturbance to the fluvial system by repeated volcanic damming (evidenced by lake sediments draped across the younger terraces) , lake drainage and the influx of volcanic products during this interval (Maddy *et al*., 2012b).

Since 2012, our extensive programme of $^{40}Ar/^{39}Ar$ radio-isotopic geochronology and palaeomagnetic measurements on critical lava flows has yielded results that require us to re-evaluate the stratigraphy published in Maddy *et al*. (2012a). Seven of these new age estimates (Figure 4a, A-G) and associated magnetic data from eight locations (Figure 4 KU1-8) were used to establish the age of a hominin artefact (Maddy *et al*., 2015) found within fluvial sediments post-dating the lava flows overlying the GT1 level sediments on Kale Tepe (Figure 3) and those same age estimates were also used in a detailed discussion of the palaeoenvironmental implications of a colluvial-fluvial sequence lying above the GT11 level on the northern limit of the Burgaz plateau (Veldkamp *et al*., 2015). Here, for the first time, we will present the full data set, which includes unpublished age estimates from six additional localities (Figure 4a, **H-M**) and six new palaeomagnetic determinations critical to our understanding of this sequence (Figure 4a, **KU9-KU14**). After describing these measurements, the implications of these new data will be discussed.

4. Establishing a refined chronology for the lava flows of the Burgaz and İbrahimağa Plateau.

4.1 Methods

Our programme of geochronological investigation involved both $^{40}Ar/^{39}Ar$ radio-isotopic measurement for age estimation and palaeomagnetic measurements focused on establishing polarity. $^{40}Ar/^{39}Ar$ measurements were undertaken at the VU University, Amsterdam and palaeomagnetic measurements at Utrecht University. Our sampling strategy was primarily designed to sample basaltic lava flows with clear stratigraphical relationships to the underlying Gediz Valley Formation or flows with a clear termination at contemporary palaeo-Gediz valley floor level. In addition, however, two samples were taken from isolated basalt boulders in attempt to establish their provenance. Sample locations for both $^{40}Ar/^{39}Ar$ (A-M) and palaeomagnetic measurements (KU1-KU14) are shown in Figure 4.

4.1.1 $^{40}Ar/^{39}Ar$ sampling and procedures

Groundmass separates were prepared using a well-established methodology which is designed to obtain homogenous fragments of microcrystalline groundmass and thus minimize the potential for inherited argon within the phenocryst phases. Groundmass samples (~500 – 700 mg) were packed in 20 mm diameter Al-foil packages, together with 9 mm diameter packages containing mineral standard FC sanidine. This standard has a recalculated K/Ar age of 28.201 Ma (Kuiper *et al.*, 2008). Only sample K has been packed with mineral standard DRA-1 sanidine. Sample containers were packed in a standard Al-irradiation capsule and irradiated for 1 h in a Cd-lined rotating facility (RODEO) at the Petten High Flux Reactor in The Netherlands. Samples were then loaded onto a 65-mm sample tray with 5 machined depressions (3 mm deep and 17 mm wide) and placed in a vacuum house with a 50 mm diameter multispectral ZnS window. Incremental heating was done by defocusing a CO_2 laser beam to a ~2 mm straight bar using an industrial scanhead with a triangular deflection current frequency of 200 Hz. Samples were evenly heated by applying a fine x-y raster pattern over each of the sample positions. Measurements were done using a quadrupole mass spectrometer (Schneider *et al*., 2009). Mass spectrometer runs consist of stepwise measurement of the argon mass spectrum from m/e 36 to m/e 40, where on m/e 36, 39 and 40 seven readings were taken at 0.05 m/e intervals on the flat peak top, and for m/e 37 and 38 one single reading was taken. The baseline was measured at m/e 35.45. Beam signals for all peaks were measured using a pulse counting SEM detector. Aliquots of

air are measured routinely during the measurement programme to monitor mass discrimination (Wijbrans *et al*., 2011). Detailed results from these analyses are provided in supplement S1. $^{40}Ar/^{39}Ar$ ages were calculated with the freeware software package ArArCalc (Koppers, 2002), which follows standard protocols for uncertainty calculation. For presenting Quaternary basalt groundmass samples we quote the uncertainties at a one sigma level.

4.1.2 Palaeomagnetic sampling and procedures

A total of 96 samples from 14 lava sites (KU1 – KU14, Figure 4a) on the plateau were collected using a water-cooled, gasoline-powered, motor drill. Results of sites KU1 through KU8 have been shown and discussed in Maddy *et al*. (2015), here we provide the results of sites KU9-14. Samples were oriented with a magnetic compass and all magnetic measurements were corrected for the present-day declination of ~4°. All samples were stepwise progressively demagnetized up to 100 mT with alternating field (AF) increments of 5 – 10 mT. After each step, the remaining natural remanent magnetization (NRM) of the specimens was measured on a 2G Enterprises horizontal DC SQUID magnetometer (noise level 3×10-12 Am2), interfaced with an in-house developed robot-assisted automated measuring device at the Paleomagnetic Laboratory 'Fort Hoofddijk' of Utrecht University (The Netherlands). Initial NRM intensities typically range from 0.5 to 2.0 A/m, at the upper end of the dynamic range of the instrument (lightning-affected samples go up to ~75 A/m). For interpretation, demagnetization diagrams of the NRM were plotted on orthogonal vector diagrams (Zijderveld, 1967). When vector end-points showed a trend towards the origin of the diagram, we determined this component to be the characteristic remanent magnetization (ChRM). ChRMs were calculated with principal component analysis (Kirschvink, 1980). Because the plateaus where the samples were collected are prone to lightning strikes, which create magnetic overprints, samples were collected over an area of several tens of square metres to increase the chance that lightning-induced overprints have different directions in different samples. Where a magnetic overprint led to overlapping demagnetization spectra between two components we used the great-circle approach of McFadden and McElhinny (1988) to resolve the ChRM direction from the great circles defined by the two components for individual specimens from the same site. If the overprint

direction is not everywhere the same, the ChRM direction can be deduced by the common intersection point of all great circles obtained from a lava site, with two solutions (one normal, one reversed), whereby the polarity is determined by non- or only weakly overprinted samples within the same site. With the radiometric age of the flows known, magnetic polarities indicated by the ChRM directions were checked for being consistent with the geomagnetic polarity timescale (APTS 2012: Hilgen *et al*., 2012). Detailed results from these analyses are provided in supplement S2.

4.2 Results

Summary data for the $^{40}Ar/^{39}Ar$ radio-isotopic measurements and calculated age estimates are shown in Table 2. Summary data for the palaeomagnetic measurements are shown in Table 3. In order to simplify discussion sample results will be discussed with respect to location but, where possible, in stratigraphical order. All sample locations are shown on Figure 4a.

4.2.1 $^{40}Ar/^{39}Ar$ radio-isotopic measurements

*Sites **H**, **I** and **J** (İbrahimağa plateau)*

The oldest age estimates within our current data set come from the İbrahimağa plateau. Two samples from location **H** yielded separate age determinations of 1097 ± 99 ka and 1470 ± 97 ka respectively (Table 2). However, taken together, these samples yield a mean age of 1272 ± 80 ka. These estimates have very large uncertainty (see supplement S1). The base of the sampled outcrop lies at ~490m a.m.s.l. and the underlying Ahmetler Formation is observed in an immediately adjacent outcrop. The surface topography of this lava flow suggests a derivation from the east, higher up on the İbrahimağa plateau. Although no Gediz terrace gravels are observed here, the altitude of ~490m is consistent with this flow terminating at the GT6 valley floor level (Figure 6).

Basalts sampled at locations **I** and **J** were derived from outcrops which have previously been assigned a ß3 age by Bunbury *et al*. (2001), presumably on the basis of their comparatively low altitude i.e. ~50m beneath the flows covering the adjacent plateau. Our field observations, however, could not establish a clear basal contact with the underlying

Ahmetler Formation and the outcrop terminated abruptly to the south coinciding with a modern gulley orientated in an ENE-WSW direction. Based upon these observations we interpret this outcrop as a newly recognised volcanic neck referred to here as Akçeşme (no. 8, Figure 3). The age determinations of 1327 ± 11 ka (**I**) and 1298 ± 13 ka (**J**) suggest this basalt originated during the earliest phase of volcanism on the İbrahimağa plateau (Table 2). This age assignment cannot be readily dismissed. There is no obvious linkage, other than height, for this outcrop with ß3 lava outcrops further east. The obvious height difference, with no evidence of displacement of the basalt, does however require explanation (see below).

Sites A, B (Burgaz plateau)

Although eruptions in the vicinity of the current İbrahimağa plateau appears to be the earliest eruption centres, they are quickly joined by eruptions from Burgaz Bağtepe. Basalts from location A yielded an age estimate of 1297 ± 17 ka (Maddy *et al*., 2015). This sample lies directly above a thick colluvial sequence described by Veldkamp *et al*. (2015), which in turn overlies GT11, the highest Gediz terrace thus far recognised. The palaeo-Gediz valley towards which this lava most likely flowed is indeterminate as it merges with more recent flows south of the outcrop. Basalt sampled at location B yielded an age estimate of 1287 ± 25 ka (Maddy *et al*., 2015), which may or may not represent the same lava flow as A.

*Site **K** (isolated boulder)*

A large isolated block of basalt at location **K** yielded an age estimate of 1325 ± 43 ka (Table 2). The location and age of this boulder suggests it is derived from one of the earliest eruptions. This could be an isolated remnant of a lava flow largely removed by subsequent erosion or possibly it is associated with the post- Lake 1 lake lava flow which caps the Çakırca sequence dated by Westaway *et al*. (2006) to 1264 ± 16 ka.

Sites Ci, Cii, D and E (Burgaz plateau)

Maddy *et al*. (2015) reported a series of age estimates from the southern sections of the Burgaz plateau where the lavas cover the deposits of GT5-GT1. Samples from Kale Tepe at Ci and Cii yielded age estimates of 1266 ± 18 ka and 1251 ± 25 ka respectively and when

considered together these yield an estimate of 1256 ± 16 ka (Table 2). The Kale Tepe lava lies above GT1. A further sample from location D yielded an estimate of 1241 ± 9 ka, Maddy *et al*. (2015) considered this to be from the same lava flow that caps Kale Tepe and thus combined all of these ages to derive an overall estimated mean age of 1247 ± 8 ka for the flow. Continuing eruption of the Burgaz Bağtepe volcanic neck is supported by an age estimate from lava location E, which yields an estimate of 1170 ± 9 ka. It is indeed possible that further eruptions continued well beyond this time as Westaway *et al*. (2006) report an age estimate of 1014 ± 23 ka from a lava sample taken south-east of the Burgaz Bağtepe volcanic neck.

Sites F and G (Delihasan)

Maddy *et al*. (2015) report samples from locations F and G, which relate to eruption from the Delihasan volcanic neck (Figure 3). These yielded age estimates of 1255 ± 17 ka and 1240 ± 60 ka respectively (Table 2). The ages support contemporaneous activity of the Burgaz Bağtepe and Delihasan necks. Although sample F is taken from lava that overlies GT4 on Ziftçi Tepe (Figure 3), it is unclear whether that flow terminated at that level.

*Sites **L** and **M** (İbrahimağa plateau)*

The youngest lava flow age estimates reported here all come from the İbrahimağa plateau. Flows emanating from the İbrahimağa Bağtepe volcanic neck flow both west and east around the earlier Tavşan flows. A flow to the west of Tavşan (**L**) yielded an age estimate of 1082 ± 15 ka and samples from a flow east of Tavşan (**M**) yielded age estimates of 1101 ± 19 ka and 1018 ± 19 ka, which when combined, yield a mean age of 1069 ± 16 ka (Table 2). These age estimates are consistent with the previously published age estimate of 999 ± 21 ka from İbrahimağa east (Westaway *et al*., 2006). All of these lavas flow across, and thus post-date, the mapped Gediz terrace outcrops beneath them. The deep incision of the adjacent modern Gediz may have been partially responsible for the widespread landsliding observed to the north of the plateau (Ozaner, 1992). Thus, although fragments of these lava flows can be traced at lower levels, their position is more likely to result from mass movement rather than primary deposition masking their relationship to any contemporary valley floor.

4.2.2 Palaeomagnetic Measurements

Demagnetization diagrams typically demonstrate the presence of one magnetic component that decays towards the origin. Initial NRM intensities were very high, between 1 and 75 A/m, as expected for basaltic lavas. The upper end is indicative of being influenced by lightning strikes. Typical demagnetization diagrams are given in Supplemental S2; site average directions and statistical parameters are given in Table 3. Many samples experienced gyro-remanent magnetization at demagnetization steps beyond 25-30 mT (Dankers and Zijderveld, 1981). This did not influence the determination of the magnetic polarity, and where demagnetization steps below 30 mT typically already converged towards the origin, and were consequently interpreted as the ChRM without applying great-circle analysis. Some samples of sites KU9, 11, and 13 clearly showed two simultaneously decaying components, one with varying orientations (the lightning-induced NRM component) and one common among all samples.

Averages and statistical parameters of each lava site was determined by Fisher (1953) statistics. All lava sites have a Fisher precision parameter k well exceeding 50 (Table 3), which is normally taken as the lower-bound cut-off value for a reliable spot reading of the geomagnetic field (Biggin *et al*., 2008; Johnson *et al*., 2008). All sites yielded unequivocal reversed polarities (Table 3, supplemental S2).

Since lavas cool very quickly, they represent a spot reading of the palaeomagnetic field direction and should not average palaeo-secular variation (PSV). PSV results in short-term magnetic field direction variations and the directions measured in a single lava site may deviate up to ~25° from the palaeomagnetic pole (i.e. the average of a certain number of flows). All sites yield declinations that are deviating clockwise from the South Pole. The sites, particularly from the Burgaz plateau, however, are very tightly clustered, much more than expected from a scatter induced by PSV (Deenen *et al*., 2011) and although the study area is tectonically active, we interpret this deviation to result from insufficient averaging of PSV rather than a tectonic rotation.

The reversed polarities are in general agreement with the geochronological results. All sampled lavas, including KU1-8 previously reported in Maddy *et al*. (2015) are thus conveniently placed within the Matuyama chron. Only sample KU14, which was sampled from a lava flow on the eastern limit of the İbrahimağa plateau, presents potentially contradictory evidence. This lava flow unit sampled at location O yielded a mean age of 1037± 12 ka which would place this lava in the Jaramillo normal subchron (~0.99 – 1.07 Ma, spanning across MIS31-27). There, however, exists a reversed event within this subchron, the so-called Intra-Jaramillo Event (Laj and Channell, 2007; Ao *et al.*, 2012). Somehow fortuitous, it could be that the KU14 flow was emplaced during that time span, at least the ages would correspond.

4.3 Conclusions from the new geochronological investigation

The results of our geochronology investigation provide a clearer picture of the sequence of eruptions during the Early Pleistocene phase of volcanism within the Kula Volcanic Province. These new age data suggest that our previously published chronology for the Gediz terrace sequence (Maddy *et al*., 2012a) requires further revision. For the first time:

i. We have been able to establish an absolute age for the earliest eruptions of the İbrahimağa plateau, which appear to cause the damming of the Gediz River at the level of GT6. This valley floor was active immediately prior to the first eruption at ~1320 ka. It is likely therefore that the GT6 sediments were deposited during MIS42. Attribution of ages to the higher GT7-11 terraces must therefore pre-date this event and will be discussed below;

ii. The age of the lava flow capping the lowest GT1 Gediz terrace deposits on Kale Tepe suggests GT1 must pre-date ~1247 ka (Maddy *et al*., 2015), which is time-equivalent to MIS38. This age assignment confirms that terraces GT5 – GT1 were deposited during the period ~1320 ka - ~1247 ka (MIS42 – MIS38). During this period, eruptions occurred both upstream from the Delihasan volcanic neck and downstream from the Kavtepe, Toytepe and Sarnıç Bağtepe (Sarnıç plateau), and Tavşan (İbrahimağa

plateau) volcanic necks.

In addition:

iii. We have confirmed that volcanic activity continued sporadically until at least ~1Ma (MIS28) on the İbrahimağa plateau.

Neotectonics: Recent Field Observations

The presence of significant neotectonic E-W trending fault structures in the Selendi Basin immediately north of the study area (Purvis and Robertson, 2004, Figure 2) and the knowledge that tectonic extension is still ongoing, makes it curious that previous work (including our own) has found no evidence of faulting during the Quaternary; furthermore no Plio-Quaternary E-W orientated faults have been reported in the literature for our field area. Nevertheless, during the course of sampling for our most recent geochronology, several key new observations were made around the İbrahimağa plateau that suggest fault movement may have played a more significant role in landscape evolution during Plio-Quaternary than has previously been recognised. The observations have a bearing on the use of this new chronology and our understanding of the Quaternary stratigraphy.

5.1. Plio-Quaternary Fault Movement

Evidence for ENE-WSW orientated structures in the study area (parallel to the strike of the Alaşehir graben faults, see Figures 1, 2) can readily be identified using aerial images such as those in Google Earth. Here we use a higher resolution monochromatic satellite (Alos Prism) stereo image pair to produce a high-resolution (3m) digital elevation model (DEM) for the study area in order to identify general relief patterns. Ground control points for elevation were obtained using a Sokkia Radian IS dual frequency dGPS system. A generalized (10m) version of this high-resolution data set is used in Figures 7 (shaded DEM) and 8 (DEM).

The shaded DEM (Figure 7) shows clearly the abrupt topographic change that delimits the Ulubey Fm. limestone uplands (lineament *L1*) to the north and the dissected Ahmetler Fm. landscape to the south. Numerous faults can be observed along this marked topographic scarp. All have relatively minor offset (<20m) with downthrow to the south. Additional,

similarly aligned lineaments can be identified further south using volcanic neck alignment, outcrops of travertine, linear gulley development, straight (guided) segments of the current river path and truncated basement highs. Figure 6 shows only the most prominent lineaments. Significantly these features cut across all the strata including the ophiolites. They do not therefore signify differential erosion of bedding structures. Although evidence to support a faulting origin for *L1* is unequivocal, establishing corroborating evidence in the field to support a structural i.e. faulting origin, for all of these lineaments is more problematical given the unconsolidated nature of much of the current surface strata. Nonetheless, observations of block offset in the Ulubey Fm. between lineaments identified around the İbrahimağa plateau (e.g. *L3*, Figure 7) strongly support their association with normal faulting with downthrow to the south.

Figure 7 displays more detailed field observations around the İbrahimağa plateau. This interpretation is based upon the mapped heights of isolated *in-situ* outcrops of Ulubey Fm. limestone (*see* supplement S3 for photos of locations a-c). The ideal target for determining relative movement is the Ahmetler Fm. / Ulubey Fm. contact, as this is marked by a clear lithological change. The contact is best observed immediately west of the İbrahimağa Bağtepe volcanic neck at point a (Figure 8) adjacent to the base of the scarp cut into the Ulubey Fm. Here we measured a contact height of ~620m a.m.s.l. On the plateau, this contact is largely obscured but there is one isolated outcrop immediately west of the Tavşan volcanic neck at location b (Figure 8) where Ulubey limestone is observed *in-situ* at heights above ~580m a.m.s.l. (the base is obscured by lava which surrounds this knoll), suggesting an offset ≥40m from location a. Further north and west, at a level below the basaltic plateau, there is a further *in-situ* outcrop of Ulubey limestone at location c (Figure 8). Again the lower contact is not observed but the lowest observed level in limestone is ~510m a.m.s.l., suggesting a ≥70m offset from b (note this is the localized expression of lineament *L3* in Figure 6). Taken together, these identified offsets correspond closely with the blocks delimited by the lineaments (Figure 8) and lend support to their interpretation as normal faults with downthrow to the north.

If we accept this interpretation, some of the more troublesome observations become more readily explained. The thick (>50m) sequence of lavas overlying water-lain sediments which outcrop west of Şeremet (Figure 8, *see* Maddy *et al*., 2012a) lie ~70m below the level of the İbrahimağa plateau. In this interpretation, this exposure lies in the hanging wall of a normal fault (*f3*), which most likely formed a prominent scarp prior to lava emplacement. The lavas here and beneath Eriklikas (Figure 8) appear to infill the block defined by *f3* to the south and *f4* to the north. Indeed, the lavas of Eriklikas are truncated by *f4*, which may suggest some movement on this fault post-dates lava emplacement (see below). The basalts at location I (Figure 4a) appear to emanate from the Akçeşme volcanic (no. 8, Figure 8) fed directly through the *f4* conduit. The age data for this sample suggest *f4* was the first conduit utilised, feeding the volcanic neck 8 (Akçeşme) with volcanic neck 1 (Tavşan) fed via conduit *f2*. The oldest lava flows appear to drape across *f3* and we have, thus far, not observed any evidence to support offset of the lavas themselves. Hence it is likely that all movement along this fault had ceased prior to arrival of the Pleistocene lavas.

Given that *f3* movements are complete prior to the arrival of the earliest basalts it is likely that faults *f2* and *f1* also pre-date the volcanism. Faults *f2* and *f1* both appear to act as conduits for volcanic necks 1 and 2 respectively. As the basalts post-date faults *f1-f3*, the age of the basalt does not provide any indication of the relative age of the faults themselves. However, it is likely, given their orientation, that they are associated with the Plio-Pleistocene movements. Fault *f4* is the only fault to be directly observed at outcrop and interpretation of this exposure suggests the latest movement on this fault may be contemporaneous with the volcanism (see below).

5.1.1 Quaternary Fault Movement

Exposures at location d (Figure 9), west of the İbrahimağa plateau (Figure 8), reveal a high-angle fault with drag-structures in the sediments of the footwall indicating normal fault motion. The presence of basalt-rich sediments in the hanging wall confirms a Quaternary age for burial of this structure. The fault lies parallel to the path of the lineaments suggested in Figure 6. The fault is represented by a sharp contact with no evidence of prolonged

surface exposure, suggesting the hanging wall sediments rapidly buried the fault following displacement. The exposure is ~3m high but may have a partially eroded top.

An outcrop immediately north at location e (Figure 8) shows evidence of disturbance i.e. acute tilting of beds including Gediz gravels. Although previously attributed to mass-movement (Maddy *et al.*, 2012a), it is entirely possible that these movements were triggered by displacement on the adjacent fault. Projecting this possible fault direction westwards suggests alignment with abrupt truncations of the lava flows. These truncations are surprisingly linear, which may support a fault guided origin. Active movement on Quaternary age faults may also be responsible for the landslides immediately north of Eriklikas (Figure 8). The rapid burial of the fault suggests it is entirely conceivable that this Pleistocene fault movement on *f4* is simultaneous with one of the eruptions, and was perhaps triggered by it.

5.2 Implications of Plio-Quaternary Neotectonics

The identification of active faulting in the study area during the Plio-Quaternary has significant implications for fluvial system evolution. In Figure 7, we speculate how these movements may have exerted control on the landscape immediately prior to the onset of volcanism. The overall structure appears to be a ~10km wide graben, similar in dimension and orientation to that identified to the north of the study area by Purvis and Robertson (2005). Ersoy *et al*. (2010, p227) identify what they call an 'open structure filled by volcanic centres' in this area, which they associate with extension. The location of GT11 at the northern end of the Burgaz plateau lies close to the centre of this graben, suggesting the initial drainage of the palaeo-Gediz was located along the structural axis. This geometry, if correct, may also help to explain the landscape response to lava dam construction along the northern margins of the current İbrahimağa plateau as the first eruption of the Akçeşme volcanic neck (no. 8) appears to lie directly in the centre of this drainage axis.

Fault movements add further levels of complication to establishing correlation of fluvial deposits on the basis of longitudinal profile projection. This is particularly challenging in the vicinity of the İbrahimağa plateau, where significant offsets need to be negotiated by the

palaeo-Gediz river once its path strays south of the structural axis upstream i.e. during GT10-1. Pleistocene fault movement could also have played a role in lowering local base level with vertical displacements along the faults providing a plausible trigger for terracing.

Our investigations of Plio-Quaternary fault movements are on-going and considerable additional effort will be needed to confirm the geometry and timing of these movements. Landscape patterns and preliminary observations are strongly suggestive of structural control beyond the confines of the outcrops discussed but in many key areas outcrops are sparse (a likely function of their susceptibility to erosion). What is clear, however, is that significant Plio-Quaternary movement on faults is highly probable and their role in driving fluvial behaviour in this part of the Selendi Basin needs urgent attention.

5. A revised stratigraphy for the Gediz Valley Formation

The new geochronological data expose errors in the chronology of the Gediz Valley Formation as proposed by Maddy *et al.* (2012a) and therefore we here present a revised stratigraphy shown in Table 4. Pivotal changes include:

i. The recognition that the onset of volcanism associated with the GT6 level on the Burgaz plateau occurred earlier than anticipated during MIS42 (from MIS38).

ii. The burial of the lowest terrace identified on the Burgaz plateau is also assigned an older age, time equivalent to MIS38 (from MIS28), based upon the new data.

iii. Taken together, these age estimates not only make the GT5-GT1 sequence older, they also substantially compress the timescales for their development.

iv. We acknowledge that there is considerable uncertainty surrounding the relationship of the youngest eruptions on the İbrahimağa plateau to the Gediz terrace sequence. Their previous use as a minimum age constraint for GT1 is untenable.

6. Discussion and Identification of priorities for future work

The new chronology and neotectonic observations have important implications for the existing uplift-driven, climate-controlled model for terrace development. The revised stratigraphical model is shown in the context of wider environmental changes, as evidenced by vegetation and oxygen isotope records, in Figure 10

The attribution of the higher terrace sequence GT11-GT6 to Early Pleistocene climate cycles (MIS52 to MIS42) is supported by the palaeoenvironmental data derived from the overlying colluvial sequences reported by Veldkamp *et al*. (2015). The only change to our 2012 model here (and in Veldkamp *et al*., 2015), is based upon the older age assignment given to the first eruptions (MIS42). The identification of early eruptions on the İbrahimağa plateau supports our previously suggested location for the volcanic dam which caused the inundation of the upstream GT6 valley floor as evidenced by lacustrine sediments on both the Burgaz and Sarnıç plateaux. The higher terrace gravels seen at outcrop on the İbrahimağa plateau are all cut into the Ahmetler Fm. These gravels all outcrop in the footwall of faults and currently there is no reason to reject the existing correlation, however it does increase the uncertainty. It is presently unclear how the GT6 river responded to crossing the fault scarps. However, it is likely that the GT6 river flowed back onto limestone as it crossed the *f2* scarp and thus we might anticipate considerable confinement of the valley floor as it traversed the hanging wall block. This confined valley floor may have become increasingly confined as the river passed across fault *f3*. A narrow, comparatively deep, valley would have provided the perfect geometry for blockage by lavas emanating from the Akçeşme volcanic neck (no. 8).

More radical changes are required for our post-GT6 chronology and interpretation. In our 2012 model, the five post-eruption onset terraces of the Burgaz plateau (GT5-GT1) conveniently mirrored the five ‘cold’ stages of the original MIS attribution allowing us to suggest a continuing link with climate control over terrace development. Clearly, the more compressed chronology suggested by the new data (MIS42-MIS38) means this linkage can no longer be sustained. It is now acknowledged that the buried terraces GT5-GT1 are

localised to the Burgaz and Sarnıç plateaux. It is unlikely that these features maintained a consistent gradient beyond the immediate area thus rendering correlation either upstream or downstream problematical. Indeed, there are no reliable correlatives of the GT1 gravels downstream of the Burgaz plateau. This situation is further confused by the presence of post-GT1 Gediz gravels in the meander core (Table 4, M1) north of Kale Tepe (Maddy *et al*., 2015), which lie at the same altitude as the GT1 terrace deposits beneath the Kale Tepe flow. This deposit was attributed to MIS35 by Maddy *et al.* (2015), making these gravels the youngest, yet recognised, Gediz gravel attributable to this early phase of volcanism. The lack of gravel readily correlated with these lower levels on the İbrahimağa plateau and the newly recognised fault movements adjacent to that plateau make inferences concerning the likely level of equivalent valley floors downstream equivocal. The controls over terrace formation during GT5 to GT1 are thus a dynamical system response to repeated damming and subsequent drainage of lakes and now, the very real prospect of some localized fault movement.

Our work over the past 15 years has yielded considerable insight into this remarkable fluvial archive but as questions surrounding basic stratigraphy have been addressed, the complexity of the record has increased. This complexity presents new challenges and presents us with an ever increasing list of new questions. As we start a new phase of investigation into this record, several immediate foci for attention emerge:

1. Can we identify with more certainty the principal Quaternary ENE-WSW oriented fault structures both around and beyond the İbrahimağa plateau and if so can we establish a chronology for any movements along these structures and their implications for the Gediz terrace sequence?

2. Can we identify the Plio-Quaternary ENE-WSW oriented structure and determine a clearer pattern of Ulubey Fm. offset thus establishing the structural constraints on the earliest i.e. prior to and including the preserved terrace record, Gediz fluvial system and does this have implications for long term fluvial landscape models?

The faulting may not be confined to the early Pleistocene and thus the best field evidence may yet come from the younger Gediz terrace records and so a broader future research theme will also need to consider:

3. Can we identify the geometry and chronology of the Middle-Late Pleistocene Gediz fluvial archives and what does this stratigraphy tell us about controls on terrace formation and landscape evolution during this later time interval? Furthermore, do these younger deposits contain significant fossil records that can help us unravel changing environmental patterns?

Finally:

4. Our investigation of the Early Pleistocene sequence has already yielded a significant chance find of an early hominin artefact (Maddy *et al*., 2015). Taken in the context of the latest age determination of the hominin remains from nearby Kocabaş (Lebatard *et al*., 2014), these observations underline the probable significance of Western Anatolia as a dispersal route for early hominins. Could the Gediz fluvial archive provide the stratigraphical framework for deciphering this Palaeolithic archive?

We already have substantive quantities of observations that relate to these questions but comprehensive answers will only come through more detailed field observations. Over the lifetime of the Gediz River Project, we have used an array of modern tools including geo-bio-chemical tools such as isotopic and biomarker analyses. Although results from these laboratory investigations add considerable detail to interpretation, without appropriate field context, they would be of little practical use. The case for field mapping and observation remains as fundamental to our science as it ever did. Undoubtedly FLAG will continue to promote careful documenting of well-researched fluvial archives, the essential fabric for any subsequent high-tech investigation. Let us hope that our funding institutions can once again discover the need to support these critical field-based studies.

Acknowledgements

This work was supported by NERC (2001-2004) and the British Institute at Ankara (BIAA, 2005-2010) and contributed directly to their Climate Change strategic research initiative. DJJvH acknowledges ERC Starting Grant 306810 (SINK) and NWO VIDI grant 864.11.004. We would also like to acknowledge the help and support of Dr. Erdal Gümüş, general coordinator of the UNESCO recognised Kula Geopark, the first Geopark in Turkey.

References

Ao, H., An, Z., Dekkers, M.J., Wei, Q., Pei, S., Zhao, H., Zhao, H., Xiao, G., Qiang, X., Wu, D., Chang, H. 2012. High-resolution record of geomagnetic excursions in the Matuyama chron constrains the ages of the Feiliang and Lanpo Paleolithic sites in the Nihewan Basin, North China. *Geochemistry Geophysics Geosystems* 13, Q08017, doi:10.1029/2012GC004095.

Biggin, A., van Hinsbergen, D.J.J., Langereis, C.G., Straathof, G.B., and Deenen, M.H., 2008, Geomagnetic Secular variation in the Cretaceous Normal Superchron and in the Jurassic. *Physics of The Earth and Planetary Interiors* 169, 3-19

Borsi, S., Ferrara, G., Innicenti, F., Mazzuoli, R. 1972. Geochronology and petrology of recent volcanics in the eastern Aegean Sea. *Bulletin Volcanologique* 36, 473-496

Bozkurt, E. 2001. Neotectonics of Turkey—a synthesis. *Geodinamica Acta* 14, 3–30.

Bunbury, J.M., Hall, L., Anderson, G.J., Stannard, A., 2001. The determination of fault movement history from the interaction of local drainage with volcanic episodes. *Geological Magazine* 138, 185– 192.

Dankers, P.H.M., and Zijderveld, J.D.A., 1981, Alternating field demagnetization of rocks, and the problem of gyromagnetic remanence. *Earth and Planetary Science Letters*, 53, 89-92

Deenen, M. H. L., Langereis, C. G., van Hinsbergen, D. J. J., Biggin, A. J. 2011. Geomagnetic secular variation and the statistics of palaeomagnetic directions. *Geophysical Journal International* 186, 509–520

Erinc, S. 1970. The young volcanic topography of the Kula-Adala area. Istanbul Universitesi Cografya Enstitutu Dergisi 17, 7-22

Ercan, T. 1993. Interpretation of geochemical, radiometric and isotopic data on Kula Volcanics (Manisa-western Anatolia) *Geological Bulletin of Turkey* 36(1), 113-129

Ercan, E., Türkecan, A., Dnçel, A. & Günay, E. 1983. Geology of Kula–Selendi (Manisa) area. *Jeoloji Mühendisliği*, 17, 3–28 [in Turkish].

Ercan, T., Satir, M., Steinitz, G., Dora, A., Sarifakioúlu, E., Adis, C., Walter, H.-J., Yildirim, T. 1996. Characteristics of the Tertiary volcanics in Biga Peninsula, Gökçeada, Bozcaada and Tavşan island (NW Anatolia). MTA Bulletin, 117, 55–86 [in Turkish with English abstract].

Ersoy, E., Helvacı, C. 2007. Stratigraphy and geochemical features of the early Miocene bimodal (ultrapotassic and calc-alkaline) volcanic activity within the NE-trending Selendi basin, Western Anatolia, Turkey. *Turkish Journal of Earth Science* 16, 117–139.

Ersoy, Y., Helvacı, C., and Sözbilir, H., 2010. Tectono-stratigraphic evolution of the NE–SW-trending superimposed Selendi basin: Implications for late Cenozoic crustal extension in Western Anatolia, Turkey. *Tectonophysics*, 488, 210-232

Fisher, R.A., 1953. Dispersion on a sphere. *Proceedings of the Royal Society of London*. A217, 295-305

Hilgen F.J., Lourens L.J., van Dam J.A. 2012. The Neogene Period. *In*: Gradstein F.M., Ogg J.G., Schmitz M.D., Ogg G.M. (eds) *The geologic time scale 2012*, 923-978. Elsevier, 1144 pp.

Innocenti, F., Agostini, S., Di Vincenzo, G., Doglioni, C., Manetti, P., Savaşçin, M.Y. & Tonarini, S. 2005. Neogene and Quaternary volcanism in Western Anatolia: magma sources and geodynamic evolution. *Marine Geology* 221, 397–421.

Johnson, C.L., Constable, C.G., Tauxe, L., Barendregt, R., Brown, L.L., Coe, R.S., Layer, P., Mejia, V., Opdyke, N.D., Singer, B.S., Staudigel, H., and Stone, D.B. 2008. Recent investigations of the 0-5 Ma geomagnetic field recorded by lava flows. *Geochemistry, Geophysics, Geosystems* 9, Q04032, doi:10.1029.2007GC001696

Kirschvink, J.L., 1980, The least-squares line and plane and the analysis of palaeomagnetic data. *Geophysical Journal of the Royal Astrological Society*, 62, 699-718

Koppers, A. A. P., 2002. ArArCALC-software for $^{40}Ar/^{39}Ar$ age calculations. *Computers and Geosciences* 28, 605-619

Kroon, D., Alexander, I., Little, M., Lourens, L.J., Matthewson, A., Robertson, A.H.F. & Sakamamoto, T. 1998. Oxygen isotope and sapropel stratigraphy in the Eastern Mediterranean during the last 3.2 million years. In: Robertson, A.H.F., Emeis, K.-C., Richter, C. & Camamerlenghi, A. (eds) Proceedings of the Ocean Drilling Program, Scientific Results, 160, 181–189.

Kuiper, K.F., Deino, A., Hilgen, F.J., Krijgsman, W., Renne, P.R., Wijbrans, J.R., 2008. Synchronizing rock clocks of earth history. *Science* 320, 500e504.

Lebatard, A.E., Cihat Alçiçek,M., Rochette,P., Khatib,S., Vialet,A., Boulbes,N., Bourlès,D.L., Demory,F., Guipert,G., Mayda,S., Titov,V.V., Vidal,L., de Lumley,H. 2014. Dating the Homo erectus bearing travertine from Kocabaş (Denizli, Turkey) at at least 1.1 Ma. *Earth and Planetary Science Letters*, 390, 8-18

Laj, C., Channell, J. E. T. 2007, Geomagnetic excursions, in Treatise on Geophysics, vol. 5, Geomagnetism, edited by M. Kono, pp. 373–416, Elsevier, Boston, Mass.

Lisiecki, L. E., Raymo, M. E. 2005. A Pliocene-Pleistocene stack of 57 globally distributed benthic δ18O records. *Paleoceanography*, 20, PA1003, doi:10.1029/2004PA001071.

McFadden, P.L., and McElhinny, M.W., 1988. The combined analysis of remagnetisation circles and direct observations in paleomagnetism. *Earth and Planetary Science Letters*, 87, 161-172.

Maddy, D., Demir, T., Bridgland, D., Veldkamp, A., Stemerdink, C., van der Schriek, T., Westaway, R. 2005. An obliquity-controlled Early Pleistocene river terrace record from Western Turkey? *Quaternary Research* 63, 339-346

Maddy, D., Demir, T., Veldkamp, A., Bridgland, D. R., Stemerdink, C., van der Schriek, T., Schreve, D. 2012a. The obliquity-controlled early Pleistocene terrace sequence of the Gediz River, Western Turkey: a revised correlation and chronology. *Journal of the Geological Society of London* 169, 67-82

Maddy, D., Veldkamp, A., Jongmans, A.G., Candy, I., Demir, T., Schoorl, J.M., van der Schriek, T., Stemerdink, C., Scaife, R.G., van Gorp, W. 2012b. Volcanic disruption and drainage diversion of the palaeo-Hudut River, a tributary of the Early Pleistocene Gediz River, Western Turkey. *Geomorphology* 165-166, 62-77

Maddy, D., Schreve, D., Demir, T., Veldkamp, A., Wijbrans, J.R., van Gorp, W., van Hinsbergen, D.J.J., Dekkers, M.J., Scaife, R., Schoorl, J.M., Stemerdink, C., van der Schriek, T. 2015. The earliest securely-dated hominin artefact in Anatolia? *Quaternary Science Reviews* 109, 68-75

Ozaner, F.S. 1992. Detecting the polycyclic drainage evolution in Kula region (western Turkey) using aerial photographs. *ITC Journal* 1992–1993, 249–253.

Purvis, M., Robertson, A.H.F. 2004. A pulsed extension model for the Neogene–Recent E–W trending Alaşehir Graben and the NE–SW trending Selendi and Gördes basins, western Turkey. *Tectonophysics* 391, 171–201.

Purvis, M., Robertson, A.H.F. 2005. 40Ar–39Ar dating of biotite and sanidine in tuffaceous sediments and related intrusive rocks: implications for the early Miocene evolution of the Gördes and Selendi basins, W Turkey. *Geodinamica Acta* 19, 239–254.

Richardson-Bunbury, J.M., 1992. *The basalts of Kula and their relation to extension in western Turkey*. PhD thesis. Cambridge University.

Richardson-Bunbury, J.M. 1996. The Kula volcanic field, western Turkey: the development of a Holocene alkali basalt province and the adjacent normal-faulting graben. *Geological Magazine* 133, 275-83

Sarıca, N. 2000. The Plio-Pleistocene age of the Büyük Menders and Gediz grabens and their tectonic significance on N–S extensional tectonics in West Anatolia: mammalian evidence from the continental deposits. *Geological Journal* 35, 1–24.

Seyitoğlu, G. 1997. Late Cenozoic tectono-sedimentary development of the Selendi and Uşak–Güre basins: a contribution to the discussion on the development of east–west and north trending basins in western Turkey. *Journal of the Geological Society of London*, 134, 163–175.

Seyitoğlu, G., Anderson, D., Nowell, G., Scott, B., 1997. The evolution from Miocene potassic to Quaternary sodic magmatism in western Turkey: implications for enrichment processes in the lithospheric mantle. *J. Volcanol. Geotherm. Res.* 76, 127–147.

Schneider, B., Kuiper, K., Postma, O., Wijbrans, J.R., 2009. $^{40}Ar/^{39}Ar$ geochronology

using a quadrupole mass spectrometer. *Quaternary Geochronology* 4, 508-516.

Tzedakis, P.C., Hooghiemstra, H., Pälike, H., 2006. The last 1.35 million years at Tenaghi Philippon: revised chronostratigraphy and long-term vegetation trends. *Quaternary Science Reviews* 25, 3416-3430

Veldkamp, A., Candy, I., Jongmans, A.G., Maddy, D., Demir, T., Schoorl, J.M., Schreve, D., Stemerdink, C., van der Schriek, T., 2015. Reconstructing Early Pleistocene (1.3 Ma) terrestrial environmental change in western Anatolia: Did it drive fluvial terrace formation? *Palaeogeography, Palaeoclimatology, Palaeoecology* 417, pp.91-104. DOI:10.1016/j.palaeo.2014.10.022.

Westaway, R., Pringle, M., Yurtmen, S., Demir, T., Bridgland, D.R. & Maddy, D. 2003. Pliocene and Quaternary surface uplift of western Turkey revealed by long-term river terrace sequences. *Current Science* 84, 1090–1101.

Westaway, R., Pringle, M., Yurtmen, S., Demir, T., Bridgland, D.R., Rowbottom, G., Maddy, D. 2004. Pliocene and Quaternary regional uplift in western Turkey: The Gediz river terrace staircase and the volcanism at Kula. *Tectonophysics* 391, 121-169

Westaway, R., Guillou, H., Yurtmen, S., Beck, A., Bridgland, D.R., Demir, T., Rowbottam, G. 2006. Late Cenozoic uplift of western Turkey: Improved dating and numerical modelling of the Gediz river terrace staircase and the Kula Quaternary volcanic field. *Global and Planetary Change* 51, 131-171

Wijbrans, J. R., Schneider, B., Kuiper, K., Calvari, S., Branca, S., De Beni, E., Norini, G., Corsaro, R.A., Miraglia, L. 2011. $^{40}Ar/^{39}Ar$ geochronology of Holocene basalts; examples from Stromboli, Italy. *Quaternary Geochronology* 6, 223-232

Yilmaz, Y., Genc¸, S.C., Gqrer, F., Bozcu, M., YVlmaz, K., KaracVk, Z., Altunkaynak, X., Elmas, A., 2000. When did the western Anatolian grabens begin to develop? In: Bozkurt, E., Winchester, J.A., Piper, J.D.A. (Eds.), Tectonics and Magmatism in Turkey and the Surrounding Area. Geol. Soc. London, Spec. Publ., vol. 173, pp. 353– 384.

Yilmaz, Y., Genc¸, S.C., Karacik, S., Altunkayak, S., 2001. Two contrasting magmatic associations of NW Anatolia and their tectonic significance. *J. Geodyn.* 31, 243– 271.

Zijderveld, J.D.A., 1967, A.C. demagnetisation of rocks: analysis of results. In Collinson, D.W., and al., e., eds., *Methods in palaeomagnetism*: Amsterdam, Elsevier, p. 254-286

Figure Captions

1. General Location of the study area in Western Anatolia, Turkey. Inset shows location of Turkey within the Mediterranean Basin. TP is Tenaghi Philippon. Also shown is location of ODP967 (Kroon *et al*., 1998). Dashed box shows approximate location of Figure 2. Background image is the ASTER Global Digital Elevation Model (GDEM; ASTER GDEM is a product of METI and NASA) with heights ranging from 0 to 2400m. Grid is in UTM Zone 35 coordinates.
2. Simplified Geology of the Gediz River Basin showing the location of the Neogene Basins and their relationship to the basement rocks of the Menderes Massif. Basalts show the approximate extent of the Kula Volcanic Province. Dashed box shows the approximate position of Figure 3.
3. Generalised geology of the study area (based on Ercan *et al*., 1983 with modifications). Coordinates are UTM Zone 35.
4. A. Map of the buried Early Pleistocene terraces GT11-GT1 based upon Maddy *et al.* (2012a). Also shown are the sampling locations for the $^{40}Ar/^{39}Ar$ age estimates (A-M) and the palaeomagnetic sampling KU1-KU14. New samples reported here for the first time are shown in bold. A simplified section (α-β) showing the stepped Ahmetler-Gediz gravel contact (GT terrace bases) on the Burgaz plateau shown in B below.
5. Example outcrops. A. A general view of exposures along the western edge of the Burgaz Plateaux. B. GT5 gravels overlain by tributary gravel and colluvial sediments (close to $^{40}Ar/^{39}Ar$ sample B, Figure 4a). C. GT9 Gediz gravels overlain by tributary gravels and a volcaniclastic sequence (close to $^{40}Ar/^{39}Ar$ sample E, Figure 4a). D. Intercalated lacustrine and water-lain tephra on the Sarnıç plateaux (sample lies above presumed GT7 gravels just north of KU19 Figure 4a)
6. Terrace base longitudinal profiles for terraces of the Gediz Valley Formation (Maddy *et al*., 2012a). Sample points represent accurately surveyed height marking the contact between Gediz River gravels of the terraces and the underlying Ahmetler Fm. Shaded boxes signify the approximate extent of the high level basaltic plateaux.
7. Selected landscape lineaments (L1-L4) visible on the hill-shaded 10m DEM produced from an Alos Prism stereo image pair. Light green shading shows approximate extent of the Early Pleistocene basaltic plateau. The light yellow shading shows the approximate extent of the Miocene Ulubey limestone plateau. Inset dashed box shows the approximate location of Figure 7.

8. Close-up view of the 10m DEM in the area around the İbrahimağa plateau. Locations a-e represent outcrops described in the text. Lineaments L1-L4 are those identified in Figure 6. Dotted lines, together with lineament L3 represent faults (*f*1-*f*4): *f*1-*f*3 are identified using offset of the Ulubey Fm. and fault *f*4 is identified at outcrop d.
9. Early Pleistocene active fault *f*4 (location e, Figure 7). A(upper): General view with the *f*3 scarp shown in the background. B(lower): Close up view reveals drag structures in the hanging wall and the infill of basalt-rich debris in the foot wall.
10. Proposed correlation of: A) the regional pollen record from Tenaghi Philippon (Tzedakis *et al*., 2006), B) the $\delta^{18}0$ stacked record of Lisieki and Raymo (2005); C) the regional $\delta^{18}0$ record from ODP967 (Kroon *et al*., 1998) and D) the terrace base altitudes and chronology derived from Table 4.

Table Captions

1. General Cenozoic Stratigraphy of the Study Area (after Ersoy *et al.*, 2010; Maddy *et al.*, 2012a)
2. $^{40}Ar/^{39}Ar$ data summary table. Sample locations are shown in Figure 4. Samples A-G were previously published in Maddy et al., 2015. Samples H-M are new data published here for the first time.
3. Paleomagnetic results and statistical properties of the 14 sites in Kula basalts. Lat=latitude of the site; Lon=longitude of the site; Type indicates 'gc' when the site average was constructed using the great circle method of McFadden and McElhinny (1988); Na=number of samples analysed; Nc=number of sampled used to construct the site average; k/K=Fisher (1953) precision parameter for the site/VGP average, respectively; α95/A95=95% confidence limit of the site/VGP average, respectively; D=declination; ΔDx=95% confidence limit of the declination; I=inclination; ΔIx=95%. Sites 1-8, marked with *, were previously reported by Maddy et al. (2015).
4. Revised Early Pleistocene Stratigraphy of the Gediz Valley Formation. Attribution to MIS is based upon the MIS age boundaries taken from Lisieki and Raymo (2005) found at http://www.lorraine-lisiecki.com/LR04_MISboundaries.txt

Supplementary Information

1. $^{40}Ar/^{39}Ar$ info
2. Paleomagnetic procedures and data analysis.
3. Ulubey limestone outcrops on the İbrahimağa plateau

Fig 1.

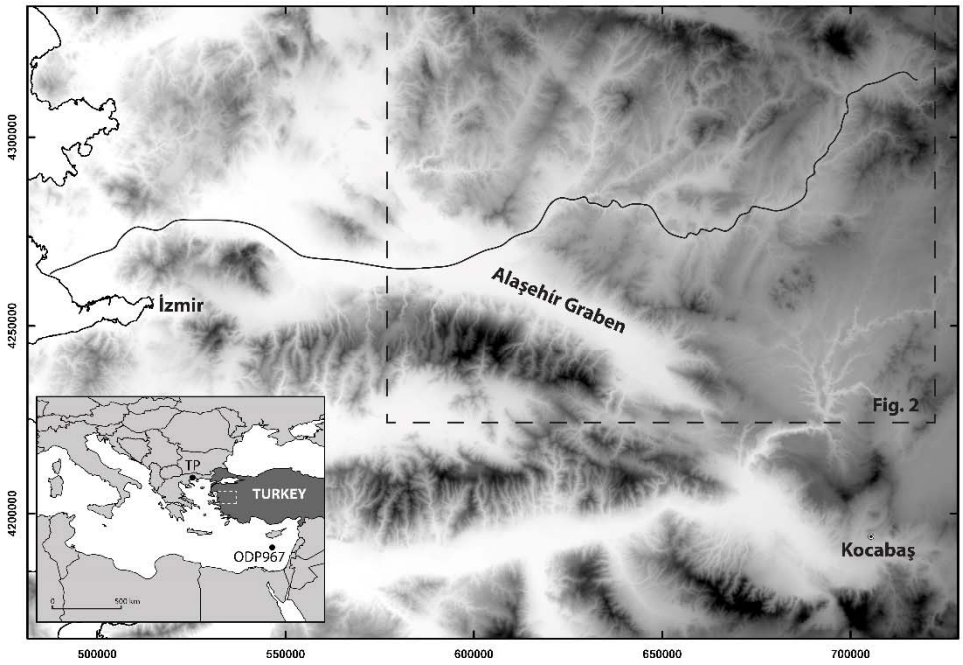
4300000
4250000
4200000
500000
550000
600000
650000
700000
İzmir
Alaşehir Graben
Fig. 2
Kocabaş
TP
TURKEY
ODP967
0
500 km

Fig 2.

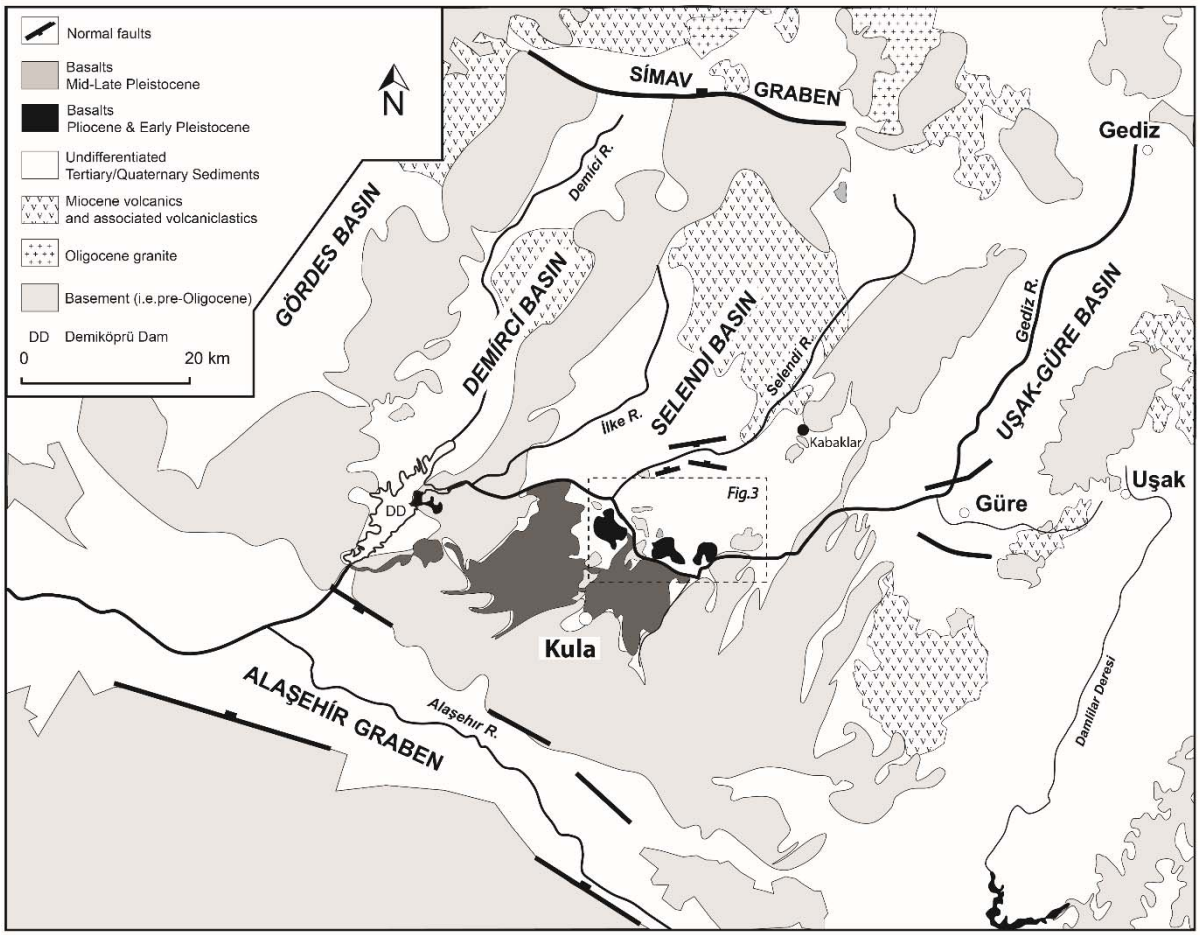
Normal faults
Basalts
Mid-Late Pleistocene
Basalts
Pliocene & Early Pleistocene
Undifferentiated
Tertiary/Quaternary Sediments
Miocene volcanics
and associated volcaniclastics
Oligocene granite
Basement (i.e.pre-Oligocene)
DD Demiköprü Dam
0
20 km
N
SİMAV GRABEN
Gediz
GÖRDES BASIN
Demirci R.
DEMİRCİ BASIN
SELENDİ BASIN
Selendi R.
Gediz R.
UŞAK-GÜRE BASIN
İlke R.
Kabaklar
Fig.3
DD
Uşak
Güre
Kula
ALAŞEHİR GRABEN
Alaşehir R.
Damlalar Deresi

Fig 3.

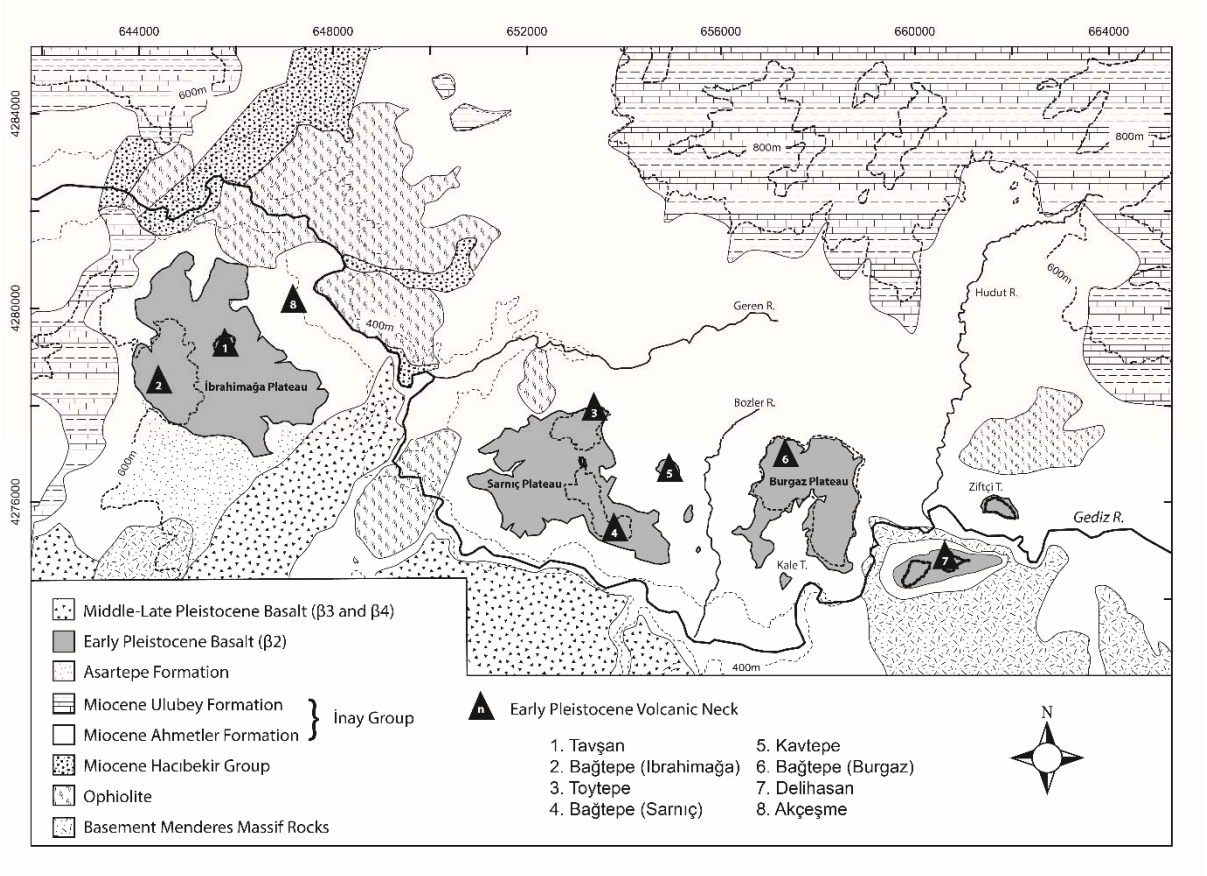
644000
648000
652000
656000
660000
664000
4284000
4280000
4276000
600m
800m
400m
Geren R.
Hudut R.
Bozler R.
Gediz R.
İbrahimağa Plateau
Sarnıç Plateau
Burgaz Plateau
Ziftçi T.
Kale T.
Middle-Late Pleistocene Basalt (β3 and β4)
Early Pleistocene Basalt (β2)
Asartepe Formation
Miocene Ulubey Formation
Miocene Ahmetler Formation
İnay Group
Miocene Hacıbekir Group
Ophiolite
Basement Menderes Massif Rocks
Early Pleistocene Volcanic Neck
1. Tavşan
2. Bağtepe (Ibrahimağa)
3. Toytepe
4. Bağtepe (Sarnıç)
5. Kavtepe
6. Bağtepe (Burgaz)
7. Delihasan
8. Akçeşme
N

Fig 4.

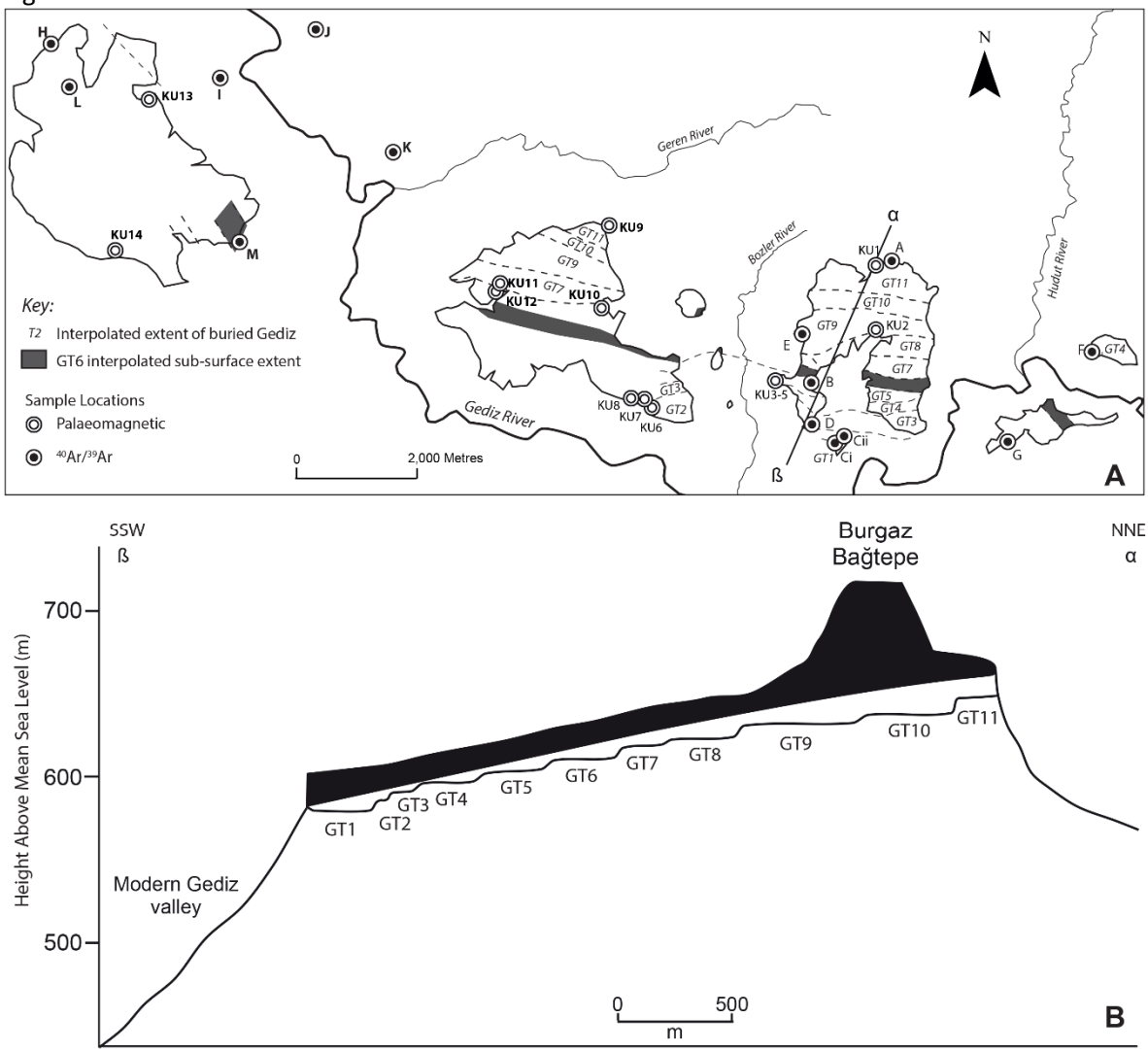
H
J
L
KU13
I
K
KU14
M
N
Geren River
KU9
GT1
GT10
GT9
KU11
GT7
KU10
KU12
Bozler River
α
KU1
A
GT11
GT10
GT9
KU2
E
GT8
GT7
B
KU3-5
GT5
GT4
GT3
D
Cii
Ci
GT1
ß
Hudut River
F
GT4
G
G13
KU8
KU7
KU6
GT2
Gediz River
Key:
T2 Interpolated extent of buried Gediz
GT6 interpolated sub-surface extent
Sample Locations
Palaeomagnetic
40Ar/39Ar
0
2,000 Metres
A
SSW
ß
Burgaz
Bağtepe
NNE
α
700
600
500
Height Above Mean Sea Level (m)
GT1
GT2
GT3
GT4
GT5
GT6
GT7
GT8
GT9
GT10
GT11
Modern Gediz
valley
0
500
m
B

Fig 5.

Fig. 6

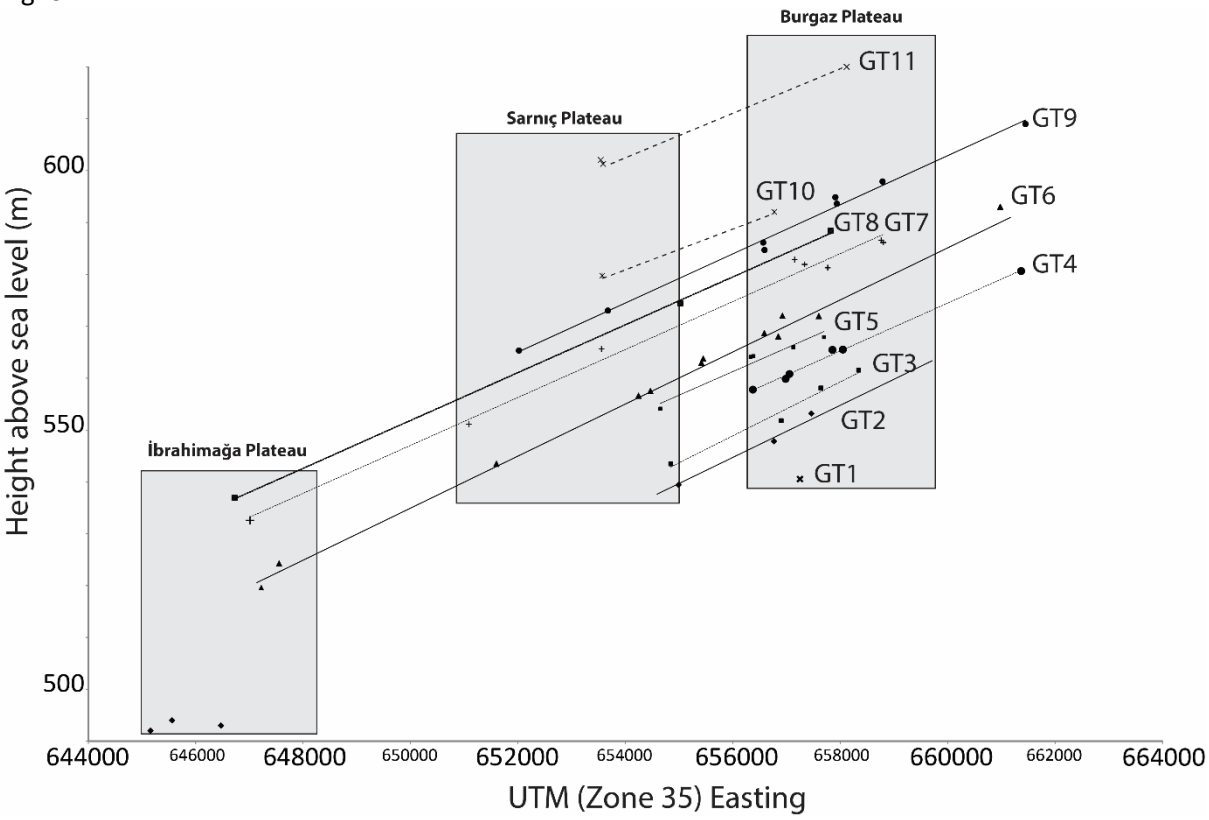
Burgaz Plateau
Sarnıç Plateau
İbrahimağa Plateau
GT11
GT10
GT9
GT8
GT7
GT6
GT5
GT4
GT3
GT2
GT1
Height above sea level (m)
600
550
500
644000
646000
648000
650000
652000
654000
656000
658000
660000
662000
664000
UTM (Zone 35) Easting

Fig 7.

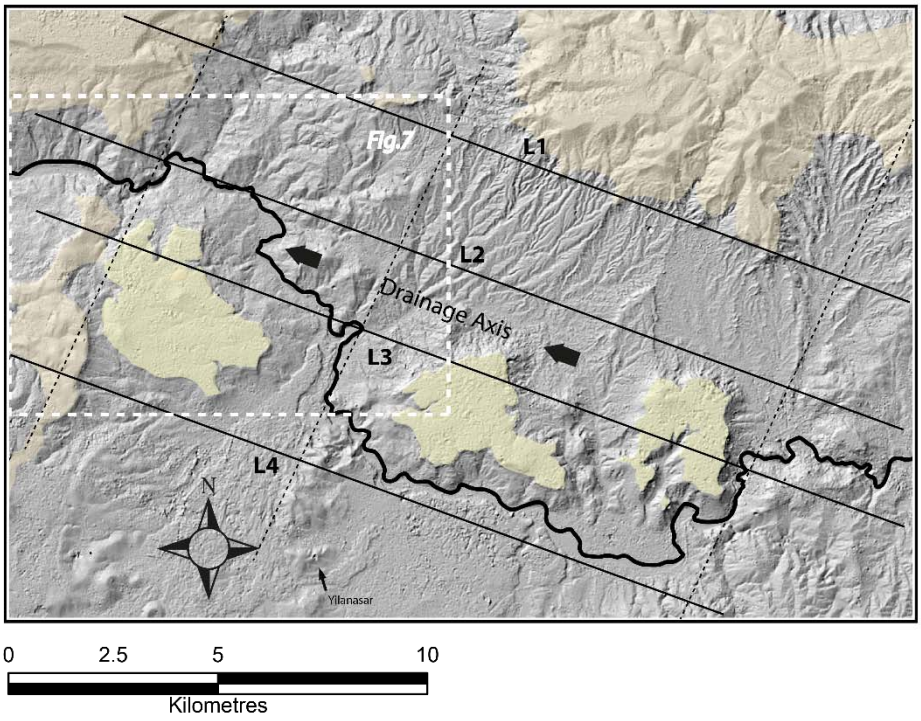
Fig.7
L1
L2
Drainage Axis
L3
L4
N
Yilanasar
0
2.5
5
10
Kilometres

Fig 8.

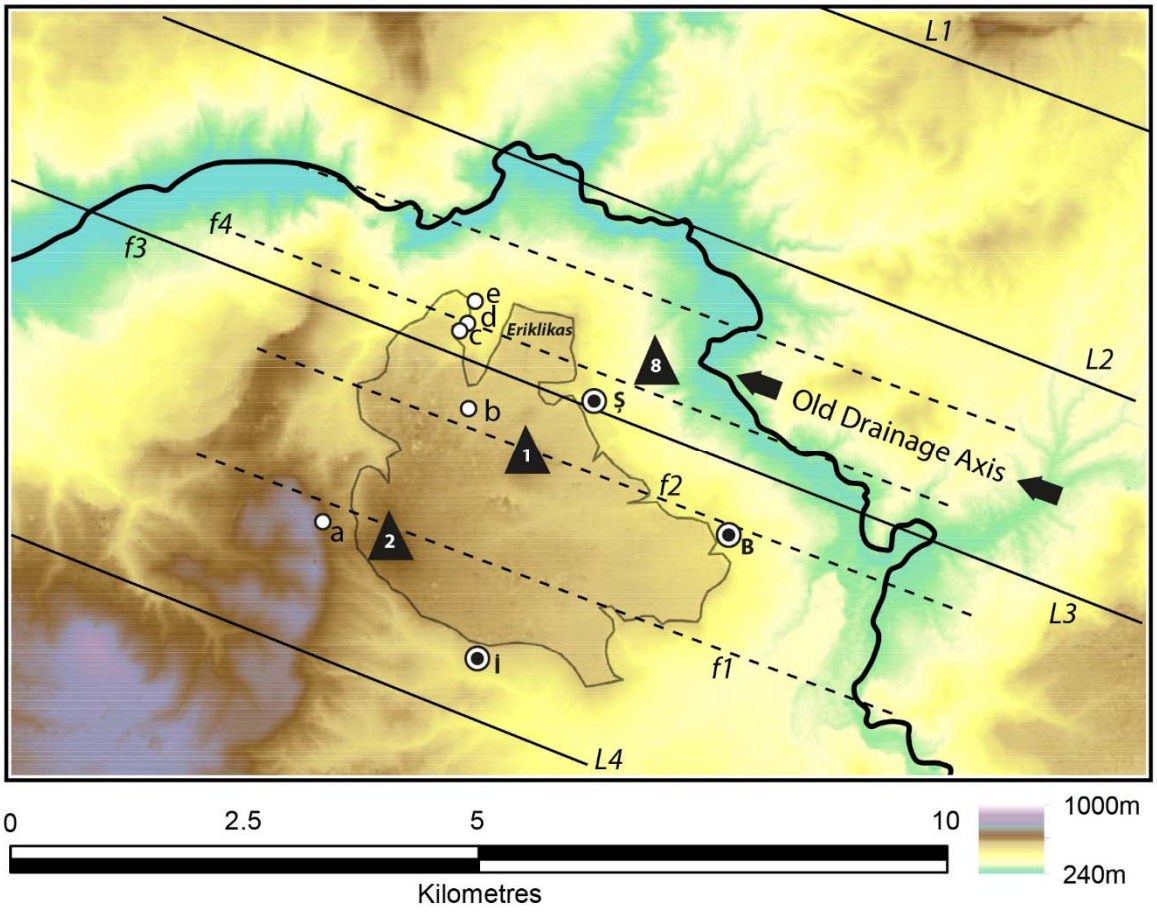
L1
L2
L3
L4
f1
f2
f3
f4
Eriklikas
Old Drainage Axis
a
b
c
d
e
ş
B
l
1
2
8
0
2.5
5
10
Kilometres
1000m
240m

Fig. 9


f3 fault scarp
f4 fault


Volcaniclastic Debris Flow
Ahmetler Fm
hanging wall
drag structures

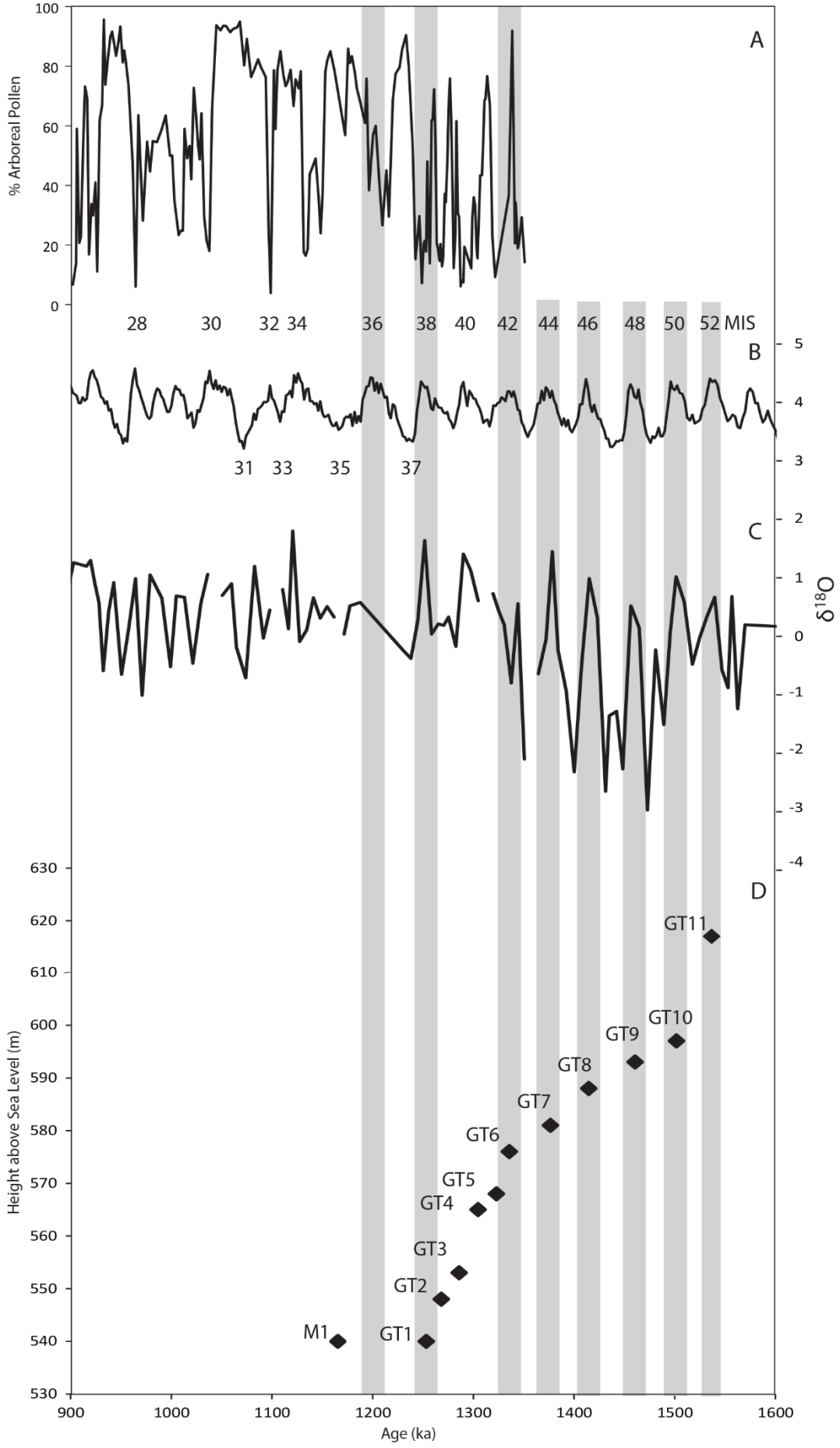
A
B
C
D
% Arboreal Pollen
100
80
60
40
20
0
28
30
32
34
36
38
40
42
44
46
48
50
52
MIS
31
33
35
37
5
4
3
2
1
0
-1
-2
-3
-4
δ18O
630
620
610
600
590
580
570
560
550
540
530
Height above Sea Level (m)
GT11
GT10
GT9
GT8
GT7
GT6
GT5
GT4
GT3
GT2
GT1
M1
900
1000
1100
1200
1300
1400
1500
1600
Age (ka)

Fig. 10

Table 1

Quaternary	Pleistocene		Gediz Valley Formation	Kula Volcanics
Tertiary	Pliocene		?Asartepe Formation	
	Miocene	Late	Kocukuz Formation	Kabaklar basalt
		Middle	İnay Group: Ulubey Formation / Ahmetler Formation	Orhanlar Basalt / Yağcıdağ Volcanics
		Early	Hacıbekir Group: Kürtköyü Formation / Yenikőy Formation	

Table 2

Name	Sample	Labcode	Plateau Age (ka)	1σ	MSWD	N. Isochron age (ka)	1σ	Inv. Isochron age (ka)	1σ
A	03E Burgaz No (above 47)	VU87 WG3_A2	1299.2	17.2	0.50	1288.3	22.1	1290.9	22.0
B	02R Burgaz west	VU87 WG2_B1	1286.9	25.2	0.71	1277.5	27.0	1280.9	27.2
Ci	W6_K2	VU94 W6_1_B1	1265.9	17.8	1.57	1180.8	53.3	1181.4	53.1
Cii	03c Kale Tepe	VU87 WG3_B1	1251.0	25.2	6.28	1263.2	29.7	1263.9	29.4
C	Ci and Cii combined	-	1255.8	16.0	3.73	1258.8	23.0	1259.7	22.5
D	W4_BW1	VU94 W4_1_C2/ VU94W5_2_B3	1241.1	9.3	1.90	1214.1	13.4	1217.0	12.7
	C and D combined	-	1246.6	8.2	2.61	1239.4	10.6	1242.2	10.4
E	W11_BW2	VU94 W11_1_B1	1170.2	9.7	0.62	1163.8	20.6	1166.0	20.3
F	GB2 Ziftce	VU87 WG2_B3	1254.8	17.4	1.26	1242.4	18.6	1249.4	19.2
G	GB4 Delihasan	VU87 WG2_A2	1239.8	60.4	0.62	1235.2	145.1	1234.2	139.4
H	IW2	94W5_1_C2	1097.9	98.8	2.27	882.0	165.1	901.9	144.0
		94W2_2_A2	1470..1	97.4	2.15	1153.7	355.5	1178.6	257.3
	IW2 combined	-	1497.6	70.8	1.97	1048.8	277.7	1066.8	187.0
I	645	94W9_1_C2	1327.0	11.0	0.65	1280.9	35.7	1281.2	35.4
J	653	94W10_1_B3	1297.1	13.4	0.53	1270.8	20	1274.1	19.4
	645/653 combined		1315.0	8.5	0.7	1274.3	16.8	1276.8	16.5
K	349	WG3_C2	1324.6	42.4	1.07	1284.1	64.2	1287.4	64.5
L	IW1	94W8_1_B2	1082.0	14.7	1.40	1003.4	22.0	1005.3	21.8
M	IE1	94W1_1_B1	1101.8	18.8	1.48	1041.9	25.8	1043.8	25.6
		94W4_3_C2	1017.9	19.3	0.53	998.1	44.7	999.2	44.6
	Combined IE1	-	1069.0	15.8	1.72	1010.0	18.3	1013.4	18.3

Table 3

Locality Lava / neck site	Lat	Lon	Type	Na	Nc	Tilt Corrected D	ΔDx	I	ΔIx	k	K	α95	A95	polarity
Kula: all				***14***	***12***	***199.1***	***12.8***	***-64.9***	***6.7***		***25.7***		***8.7***	***reversed***
KU 1	38.6301	28.8128	gc	7	7	215.8		-69.7		87.8		6.5		reversed
KU 2	38.6199	28.8133		7	6	214.0		-69.7		1446.2		1.8		reversed
KU 3	38.6129	28.7943	gc	7	6	221.7		-80.5		86.6		7.2		reversed
KU 4	38.6129	28.7943	gc	7	6	200.8		-64.1		58.8		8.8		reversed
KU 5	38.6129	28.7943		7		inconclusive: both normal and reversed. See text								
KU 6	38.6103	28.7717	gc	7	5	209.0		-69.8		108.2		7.4		reversed
KU 7	38.6102	28.7697	gc	7	7	191.4		-47.8		382.1		3.1		reversed
KU 8	38.6353	28.7660	gc	7	7	179.5		-51.5		479.2		2.8		reversed
KU 9	38.6219	28.7637	gc	7	7	236.9		-76.8		102.3		6.0		lightning
KU 10	38.6253	28.7407		7	7	182.6		-74.1		201.3		4.3		reversed
KU 11	38.6561	28.6791	gc	7	6	201.2		-69.6		251.9		4.2		reversed
KU 12	38.6561	28.6791		7	7	185.4		-60.3		119.0		5.6		reversed
KU 13	38.6561	28.6791	gc	6	5	222.6		-63.7		436.1		3.7		reversed
KU 14	38.6328	28.67685		6	6	197.1		-50.0		763.0		2.4		reversed

Table 4

Gediz Terrace	Eruption					Lakes	Age			MIS
	Ziftçi	*Delihasan*	*Burgaz Plateau*	*Sarnıç Plateau*	*İbrahimağa Plateau*		our study	published	estimated	
					İbrahimağa East			999±21		28
			Burgaz NE					1014±23		28/29
					M		**1069±16**			30
					L		**1082±15**			
			E			Lake?	1170±10			35
M1				Sarnıç Bagtepe				1174±26		
			Burgaz West (İnkale)					1186±78		
				Toytepe E				1219±27		37
		G					1239±60			
	F						1254±17			38
			D				1247±8			
GT1			CD				1246±8			
			C				1256±16			
				Toytepe W				1264±15		39
					H		**1272±80**			
			B				1286±25			40
					J		**1297±13**			
				Sarnıç Bagtepe (Maar)						
				Kavtepe		Lake L1				
			A				1299±17			
					K		**1325±42**			42
					I		**1327±11**			
GT6									1330e	
GT7									1370e	44
GT8									1420e	46
GT9									1460e	48
GT10									1500e	50
GT11									1540e	52

THE GEDIZ RIVER FLUVIAL ARCHIVE:
A BENCHMARK FOR QUATERNARY RESESARCH IN WESTERN ANATOLIA

Maddy, D., Veldkamp, A., Demir, T., van Gorp, W., Wijbrans, J.R., van Hinsbergen, D.J.J., Dekkers, M.J., Schreve, D., Schoorl, J.M., Scaife, R., Stemerdink, C., van der Schriek, T. and Bridgland, D.

Supplement 1: $^{40}Ar/ ^{39}Ar$ analysis and sample data

This supplement contains:

- Text S1. Description of geochronology sample problems
- Text S2. Geochemical characterisation
- Table S1. Volcanic rock classification based on SiO_2 and (K_2O + Na_2O)
- Figure S1. Spider diagram.

S1: Description of geochronology sample problems

The details of all samples can be accessed in the supplementary excel exports from ArArCalc. Below we discuss those samples which need some more explanation.

H: 94W5_1_C2, 94W2_2_A2

Sample 94W5_1_C2 has a near plateau age of 1097.9 ± 98.8 ka. The final three steps show signs of inheritance and are therefore omitted. However, despite relatively high step uncertainties, the plateau age MSWD value is quite high, indicating excess scatter in the individual age steps. Isochron ages do not correspond with plateau age at a 1σ but do correspond at the 95% confidence interval.

Sample 94W2_2_A2 has a near plateau age of 1470.1 ± 97.4 ka. High uncertainties of individual steps and high uncertainties of Isochron ages indicate that this age estimate is not to be used at face value.

Because the two individual results of this sample where scattered, we decided to calculate the weighted mean of the two samples. The combination of samples 94W5_1_C2 and 94W2_2_A2 yields a combined plateau age of 1272.4 ± 80.0 ka. It has a relatively high MSWD, indicating excess scatter, as well as unexpectedly young isochron ages, which may point to a regression artefact. As a consequence its age estimate should be used with caution.

S2. Geochemical characterisation of samples

Geochemistry of the samples was carried out at Activation Laboratories, Lancaster, Canada. Rock classification was done based on a TAS diagram (Total alkalis). Geochemistry points to intraplate volcanics. The non-depleted values of Nb and Ta indicate intraplate volcanics. P depletion is usually related to crystallisation of apatite from the magma chamber. No significant differences between samples are apparent.

Table S1. Volcanic rock classification based on SiO2 and (K2O + Na2O)

		Analyte Symbol-->	SiO2	Na2O+K2O	Na2O	K2O
		Unit Symbol-->	%		%	%
		Detection Limit-->	0.01		0.01	0.01
		Analysis Method-->	FUS-ICP		FUS-ICP	FUS-ICP
Name	**Sample code**	**Rock Type name**				
H	IW2	Phonotephrite	**46.69**	**8.54**	5.01	3.53
I	645	Tephrite or Basanite	**46.57**	**5.90**	4.56	1.34
J	653	Basalt	**46.36**	**4.90**	3.84	1.06
K	349	Tephrite or Basanite	**45.70**	**7.08**	4.03	3.05
L	IW1	Phonotephrite	**49.09**	**9.18**	5.64	3.54
M	IE1	Phonotephrite	**48.36**	**9.06**	5.61	3.45

Figure S1. Spider diagram. Trace element data normalized to Cl carbonaceous chondrites[7]

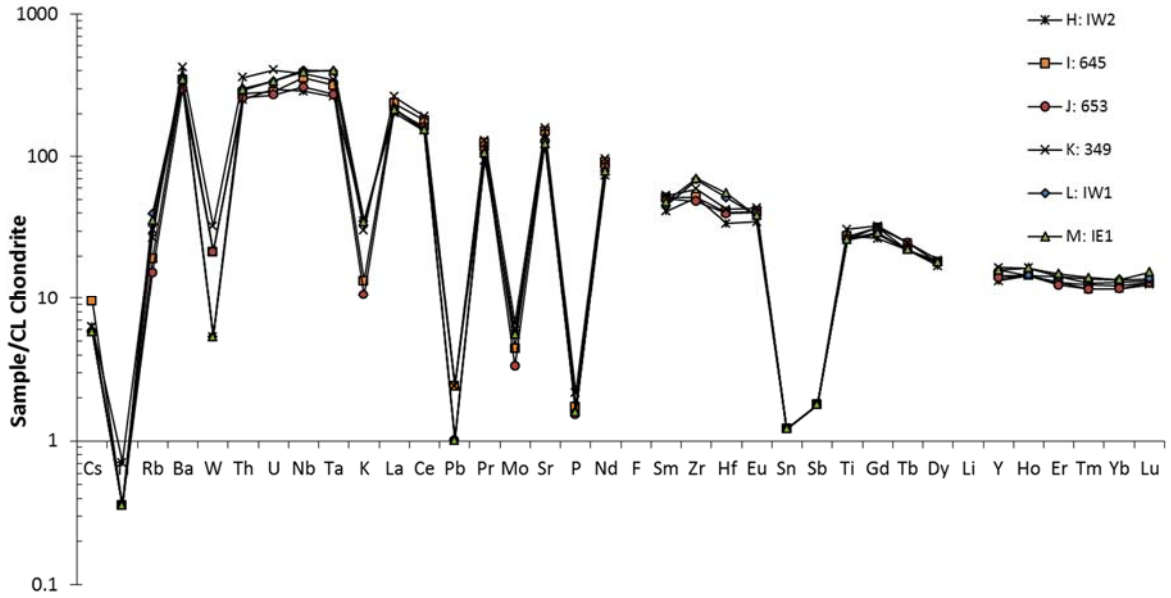

References

1 Wijbrans, J. R., Pringle, M. S., Koppers, A. A. P. & Scheveers, R. Argon geochronology of small samples using the Vulkaan argon laserprobe. *Proceedings of the Royal Netherlands Academy of Arts and Sciences* **98**, 185-218 (1995).

2 Kuiper, K. F. *et al.* Synchronizing rock clocks of earth history. *SCIENCE* **320**, 500-504 (2008).

3 Min, K., Mundil, R., Renne, P. R. & Ludwig, K. R. A test for systematic errors in 40Ar/39Ar geochronology through comparison with U/Pb analysis of a 1.1-Ga rhyolite. *Geochimica et Cosmochimica Acta* **64**, 73-98 (2000).

4 Koppers, A. A. P. ArArCALC-software for 40Ar/39Ar age calculations. *Computers and Geosciences* **28**, 605-619 (2002).

5 Lee, J. Y. *et al.* A redetermination of the isotopic abundances of atmospheric Ar. *Geochimica et Cosmochimica Acta* **70**, 4507-4512 (2006).

6 O'Connor, J. M. *et al.* Hotspot trails in the South Atlantic controlled by plume and plate tectonic processes. *Nat. Geosci.* **5**, 735-738 (2012).

7 McDonough, W. F. & Sun, S. s. The composition of the Earth. *Chemical Geology* **120**, 223-253 (1995).

Supplementary information 2: Paleomagnetic procedures and results

Paleomagnetic sampling and procedures

In addition to sites KU1-8, previously reported in Maddy et al. (2015), we here report on the analyses of an additional 40 cores from 6 lava sites in Quaternary basalts of Kula, KU9-14. Paleomagnetic sampling was performed using a water-cooled, gasoline-powered, motor drill. They were oriented with a magnetic compass and all magnetic measurements were corrected for the present-day declination of ~4°. All samples were demagnetized using alternating field (AF) progressive demagnetizations with 5 – 10 mT increments up to 100 mT. The natural remanent magnetization (NRM) of the specimens was measured on a 2G Enterprises horizontal DC SQUID magnetometer (noise level $3\times10^{-12}Am^2$). The instrument was interfaced with an in-house developed robot-assisted automated measuring device.

Demagnetization diagrams of the NRM were plotted in orthogonal vector diagrams (Zijderveld, 1967). In addition, a number of multi-component samples were plotted on equal-area projections. Initial intensities typically range from 0.5 to 2.0 A/m, with the exception of site KU 9, which had abnormally high intensities of up to 4 A/m.

On selected samples so-called acquisition curves of the isothermal remanent magnetization (IRM) were determined and the temperature dependence of the low-field magnetic susceptibility was measured to assess the magnetic minerals present in the rocks. Four samples were processed. The IRMs were imparted with a pulse magnetizer attached to the robotized SQUID magnetometer. To remain within the dynamic range of the magnetometer, chips of ~30 mg of each sample were encased in epoxy to make specimens of the required size (a cylinder of 12 mm diameter and 10 mm length). IRM was imparted in 55 steps up to 700 mT to ensure a sufficient number of data points for what is referred to as component fitting (Kruiver et al., 2001). In the IRM component fitting procedure adopted here, each component is approximated by a log-Gaussian coercivity distribution with three parameters to fit: saturation IRM (SIRM) representing the amount of that component, $B_{1/2}$ representing the midpoint of its coercivity distribution, and DP indicating the width of that distribution, also called the switching field distribution. $B_{1/2}$ provides information on the magnetic mineral while DP is an indicator of the similarity of the particle ensemble, i.e. of the crystallinity of the magnetic mineral. In particular, magnetotactic biogenic particles have a very low DP (log values of

~0.15, e.g. Kruiver and Passier, 2001; Egli, 2004) because they are almost identical. However, in the present volcanic rocks they do not occur.

In the basaltic lavas titanomagnetite, which can be variably oxidized, is the anticipated dominant magnetic mineral. Therefore susceptibility vs temperature measurements were carried out with three purposes in mind 1) to determine the magnetic ordering temperature or Curie temperature that is diagnostic of the magnetic minerals, 2) to shed light on magneto-chemical changes during warming, and 3) to constrain the interpretation of the IRM components. The measurements were done with a CS3 furnace attached to a KLY3 susceptometer (noise level $2*10^{-8}$ SI, AGICO instruments, Brno, Czech Republic). Typical signals were at least two orders of magnitude above instrumental noise level. Ca. 200 mg of fragmented rock chips was heated in air first to 400°C, cooled to room temperature followed by heating to 700°C with cooling to room temperature afterwards. Heating and cooling rates were set at 'medium', this is a rate of ~6°C/min. Because the concentration of the magnetic minerals is appreciable (c. 1 per mil if recalculated to pure magnetite, see Table A1) the paramagnetic contribution to the susceptibility can be ignored. In the corresponding figures, the susceptibility vs. temperature curves are normalized to their starting value.

Results

Rock Magnetism

Susceptibility vs temperature

The behaviour of the low-field susceptibility vs temperature indicates a titanomagnetite with a fair amount of Ti substitution (~TM70 with a minor amount of oxidation, cf O'Reilly, 1984); the Curie temperature is ~100°C (very prominent in KU9.4 B, present in KU10.2B (the latter not shown), Figure A1). Also a contribution of a magnetite-like titanomagnetite (so with a low amount of Ti substituted) is detected. The latter is indicated by a Curie temperature close to 580°C. Two flows have Ti-poor magnetite in an appreciable concentration of ~80% of the susceptibility signal, KU10.2B (not shown here). The other flows (KU9.4B, Figure A1) contain almost solely the Ti-rich phase. This phase is amenable to exsolution on annealing as demonstrated by the irreversible behaviour during cooling from 400°C. After heating up to 700°C the exsolution process continues and (almost pure) magnetite is the final result. The other phase to which the intermediate titanomagnetite exsolves, ulvöspinel, has a Néel temperature well below room temperature (-153°C) and is therefore magnetically not detected in the type of experiment performed. In KU9.4 B the final susceptibility is approximately the

starting value (~10% decrease) but the behaviour during thermal cycling is irreversible indicating chemical alteration. The return to approximately the original susceptibility value is fortuitous. The two lavas analyzed with magnetite present in large amounts showed an increase in susceptibility after annealing to 400°C which could indicate that the exsolved material at that stage is of very small, magnetically superparamagnetic, grain size, something which is in line with incipient exsolution. On further exsolution the exsolved lamellae grow in size and become indistinguishable from the originally present Ti-poor magnetite.

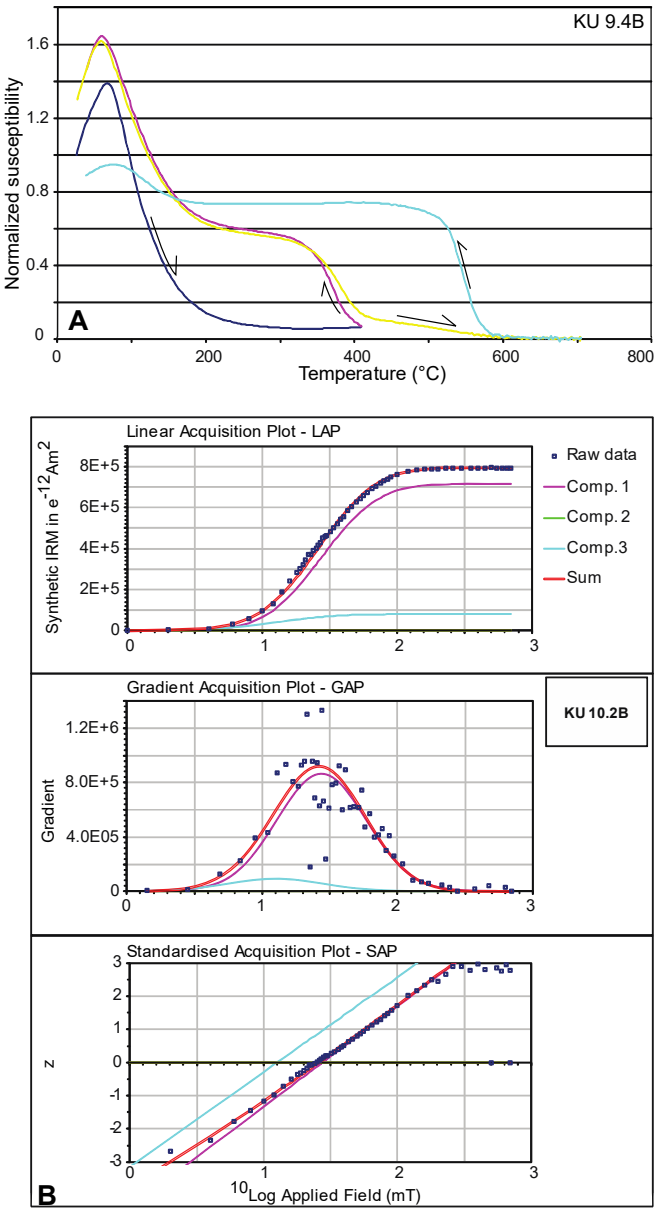

Figure A1. a). Susceptibility vs temperature behaviour for sample KU9.4B. Heating and cooling segments are indicated with arrows. All susceptibility values are normalized with respect to the starting value. Further explanation in the text.

b). IRM component fitting of sample KU 10.2B. The topmost plots are IRM measurements plotted vs log field in mT. The central panels are the gradient while the lowermost panels are standardized values of the IRM measurements. Log-Gaussian fitting was done according

IRM acquisition curves

Samples from the four flows were also subjected to so-called 'IRM component fitting' along the terminology of Kruiver et al. (2001). Logically, the IRM acquisition curves are indicating a dominant low-coercivity component. The characteristics of the fits are compiled in Table A1. Component 1 is the dominant component making 80-90% of the total IRM signal. $B_{1/2}$ is ~20-25 mT in three of the flows compatible with large pseudo-single-domain to small multidomain particles. Component 2 with a $B_{1/2}$ of 100 to 400 mT is interpreted to be

associated with Ti-rich magnetite which is magnetically hard. Dispersion parameters DP have values > 0.32 (with one exception only, Kula 9.4B) which indicates a distribution of particle sizes and Fe-Ti oxide compositions. In lavas like those investigated here the amount of Ti-substitution and oxidation of the titanomagnetites may easily vary yielding broad coercivity distributions with rather large DP values. Component 3 (not always present) is not assigned a physical meaning; in the fitting procedure adopted it is required to describe a skewed-to-the-left distribution indicative magnetic interaction or thermal activation characteristic of very small particle size (Heslop et al., 2004). In these volcanic rocks with an appreciable concentration of titanomagnetite magnetic interaction is the likely cause for the (minor) skewness. The behaviour of the low-field magnetic susceptibility and the concentration of Fe-Ti-oxides appears not to be correlated: samples with a high and low IRM show similar susceptibility behaviour.

sample	mass	component 1					component 2					component 3				
		log B1/2	B1/2	DP	IRM	fraction	log B1/2	B1/2	DP	IRM	fraction	log B1/2	B1/2	DP	IRM	fraction
	gr		mT	log units	E^-12 Am^2	%		mT	log units	E^-12 Am^2	%		mT	log units	E^-12 Am^2	%
KU 9.4B	0.03848	1.23	17	0.23	5.75E+06	82.6	1.85	70.8	0.37	4.50E+05	6.5	1.06	11.5	0.35	7.60E+05	10.9
KU 10.2B	0.03144	1.44	27.5	0.33	7.15E+05	89.9					0.0	1.1	12.6	0.35	8.00E+04	10.1

Table A1*: Results of the IRM acquisition curve fitting (Kruiver et al. 2001) of the samples processed. The total IRM is the calculated saturation IRM (SIRM) of each component added (also expressed on a mass-specific basis). Component 2 is not assigned a physical meaning (see main text). Per component the proporties are listed: Fraction (%) refers to the SIRM percentage of that component in the entire magnetic inventory; log$B_{1/2}$ is the remanent acquisition coercive force; $B_{1/2}$ is inverse logarithm; DP is the width of the*

ChRM directions

Identification of the characteristic remanent magnetization (ChRM) was done by principal component analysis (Kirschvink, 1980). When vector end-points showed a trend towards the origin of the diagram, we determined this component to be the ChRM. Samples were rejected from further analysis if the maximum angular deviation (MAD) exceeded 15°. In 9 out of 14 lava sites, an overprint induced by lightning led to overlapping demagnetization spectra between of two components. In these cases we used the great-circle approach of McFadden and McElhinny (1988) to resolve the best-fit great circle defined by the two components (Figure A2b,f). A very small amount of gyro-remanent magnetization (Dankers and Zijderveld, 1981) was observed occasionally. Because lightning overprints have random directions with respect to the NRM, the latter can be deduced by the common intersection point of all great circles obtained from a lava site (Figure A2c,g).

Only in the site KU 9 it was impossible to resolve the original direction: extremely high initial intensities of 4 A/m, together with rapid decrease of the magnetic intensity in the early demagnetization steps (compare Figure A2d with h; see also Strik et al. (2003)) are indicative of a strong lightning-induced

overprint. The steep inclination and strong deviation of the declination therefore cannot be interpreted in terms of a conclusive original polarity.

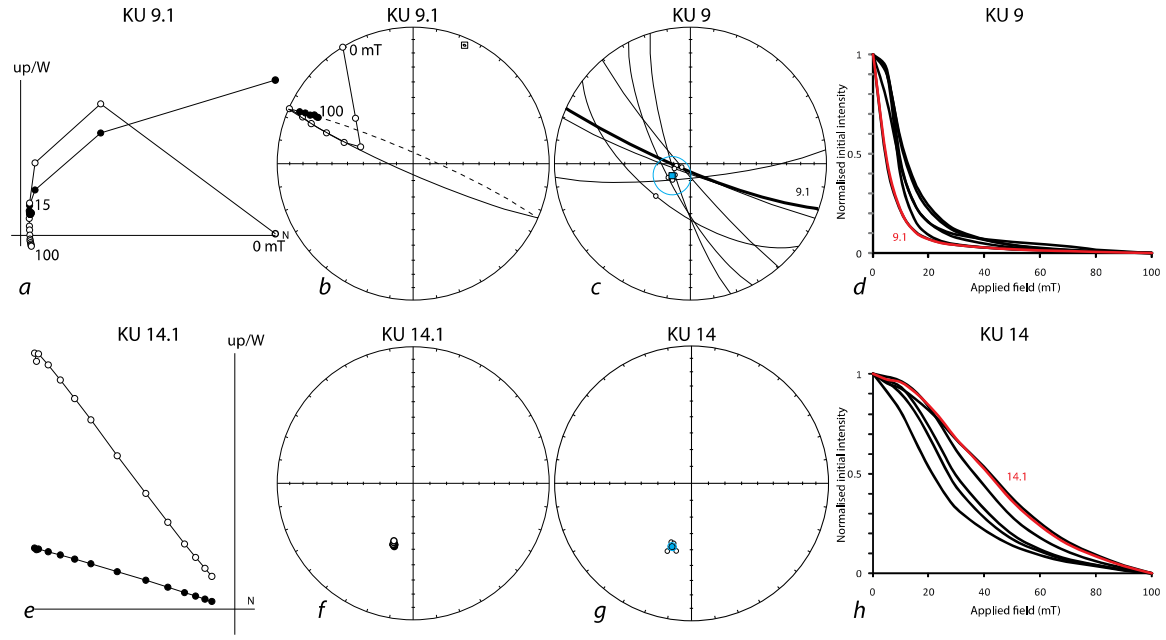

Figure A2. Representative paleomagnetic results for the Kula lavas. Left column (a, e) shows typical AF demagnetisations (steps in mT: 0, 5, 10, 15, 20, 25, 30, 40, 50, 60, 70, 80, 90, 100) on vector end-point diagrams (Zijderveld, 1967) with solid (open) symbols for projection on the horizontal (vertical) plane. Lines in (j) indicate least square line fit (Kirschvink, 1980), and (a) and (e) show simultaneous demagnetization of two components, one random and one consistent. Equal-area stereographic projection show demagnetisation path along great circle (b, f). Figures (c), (g) and (l) show typical site equal-area projection of ChRM directions in upper (open symbols) and lower (solid symbols) hemisphere, based on the common intersection point of great circles (c, g) or clustering of directions (l). Clustering of site 9 is insufficient to by-pass reliability standards of Deenen et al (2011). Right column shows decay curves, which for site 9 (Figure d) shows typical fast decay in the early demagnetization steps, in line with lighting induced remanence (Strik et al., 2003). D=declination, I=inclination, ΔD=95% confidence in

Because lava site mean directions should represent spot-readings of the Earth's magnetic field paleosecular variation (PSV), within-site errors can be assumed to be random, and averages and confidence ovals on lava site level were determined by Fisher (1953) statistics (Table 3 of main text). All lava sites have a Fisher precision parameter k exceeding 50, which is normally taken as cut-off value for reliable lava sites (Biggin et al., 2008; Johnson et al., 2008; Deenen et al., submitted). Apart from excluded site KU 9, all sites yielded reversed polarities.

Combining the 5 sites reported here with the 7 successful sites reported by Maddy et al. (2015), we obtained an average paleomagnetic direction of $D \pm \Delta D_x$ / $I \pm \Delta I_x$ 199.1±12.8 / -64.9±6.7, with K=25.7 and A95=8.7. This average was constructed applying Fisher statistics on the virtual geomagnetic poles, as scatter of paleomagnetic directions induced by PSV is ellipsoid on the globe (Tauxe and Kent, 2004;

Deenen et al., 2011). This result suggests a small but significant counterclockwise rotation, which is surprising, given the young age of the lavas, the absence of evidence for significant local deformation of the volcanic fields around Kula, and the recent notion that on a regional scale in the Selendi basin, and surrounding basins, no significant vertical axis rotations occurred since the middle Miocene (van Hinsbergen et al., 2010). It is possible that our lava sites come from a very limited time span, overrepresenting secular variation of the Earth's magnetic field (although the scatter of data is not very tight and may represent secular variation). We have no direct explanation for the deviating declination, but for the purpose of this study, it is an irrelevant issue. For chronology estimates, the most important conclusion is that our paleomagnetic results of the conclusive Pleistocene lava sites around Kula all have reversed polarity.

References

Biggin, A., van Hinsbergen, D.J.J., Langereis, C.G., Straathof, G.B., and Deenen, M.H., 2008, Geomagnetic Secular variation in the Cretaceous Normal Superchron and in the Jurassic: Physics of The Earth and Planetary Interiors, v. 169, p. 3-19.

Dankers, P.H.M., and Zijderveld, J.D.A., 1981, Alternating field demagnetization of rocks, and the problem of gyromagnetic remanence: Earth and Planetary Science Letters, v. 53, p. 89-92.

Deenen, M.H., Langereis, C.G., van Hinsbergen, D.J.J. and Biggin, A.J., 2011, Geomagnetic secular variation and the statistics of palaeomagnetic directions: Geophysical Journal International v. 186, p. 509-520.

Dunlop, D., and Özdemir, Ö., 1997, Rock Magnetism: Fundamentals and Frontiers: Cambridge, Cambridge University Press, 573 p.

Egi R. (2004). Characterization of individual rock magnetic components by analysis of remanence curves. 3. Bacterial magnetite and natural processes in lakes. Phys. Chem. Earth, v. 29, p. 869–884.

Fisher, R.A., 1953, Dispersion on a sphere: Proceedings of the Royal Society of London, v. A217, p. 295-305.

Heslop D., McIntosh G., Dekkers M.J. (2004). Using Time and temperature dependant Preisach models to investigate the limitations of modeling of isothermal remanent magnetisation acquisition curves with cumulative log Gaussian functions. Geophysical Journal International, v. 157, p. 55-63.

Johnson, C.L., Constable, C.G., Tauxe, L., Barendregt, R., Brown, L.L., Coe, R.S., Layer, P., Mejia, V., Opdyke, N.D., Singer, B.S., Staudigel, H., and Stone, D.B., 2008, Recent investigations of the 0-5 Ma geomagnetic field recorded by lava flows: Geochemistry, Geophysics, Geosystems, v. 9, p. Q04032, doi:10.1029.2007GC001696.

Kirschvink, J.L., 1980, The least-squares line and plane and the analysis of palaeomagnetic data.: Geophysical Journal of the Royal Astrological Society, v. 62, p. 699-718.

Kruiver P.P., Dekkers M.J. and Heslop D. (2001). Quantification of magnetic coercivity components by the analysis of acquisition curves of isothermal remanent magnetisation, Earth and Planetarry Science Letters, v. 189, p. 269-276.

Kruiver P.P. and Passier H.F. (2001). Coercivity analysis of magnetic phases in sapropel S1 related to variations in redox conditions, including an investigation of the S-ratio. Geochemistry, Geophysics, Geosystems, v. 2, p. 1063, doi:10.1029/2001GC000181

McFadden, P.L., and McElhinny, M.W., 1988, The combined analysis of remagnetisation circles and direct observations in paleomagnetism: Earth and Planetary Science Letters, v. 87, p. 161-172.

O'Reilly W. (1984). Rock and mineral magnetism. Blackie (Glasgow and London), 220 pp.

Strik, G., Blake, T.S., Zegers, T.E., White, S.H., and Langereis, C.G., 2003, Palaeomagnetism of flood basalts in the Pilbara Craton, Western Australia: late Archaean continental drift and the oldest known reversal of the geomagnetic field: Journal of Geophysical Research, v. 108, p. 2551, doi: 10.1029/2003JB002475.

Tauxe, L., and Kent, D.V., 2004, A simplified statistical model for the geomagnetic field and the detection of shallow bias in paleomagnetic inclinations: was the ancient magnetic field dipolar?, *in* Channell, J.E.T., Kent, D.V., Lowrie, W., and Meert, J.G., eds., Timescales of the Paleomagnetic field, Geophysical Monograph, Volume 145, American Geophysical Union, p. 101-115.

van Hinsbergen, D.J.J., Dekkers, M.J., Bozkurt, E., and Koopman, M., 2010, Exhumation with a twist: paleomagnetic constraints on the evolution of the Menderes metamorphic core complex (western Turkey): Tectonics v. 29, TC2596, doi:10.1029/2009TC002596.

Zijderveld, J.D.A., 1967, A.c. demagnetisation of rocks: analysis of results, *in* Collinson, D.W., and al., e., eds., Methods in palaeomagnetism: Amsterdam, Elsevier, p. 254-286.

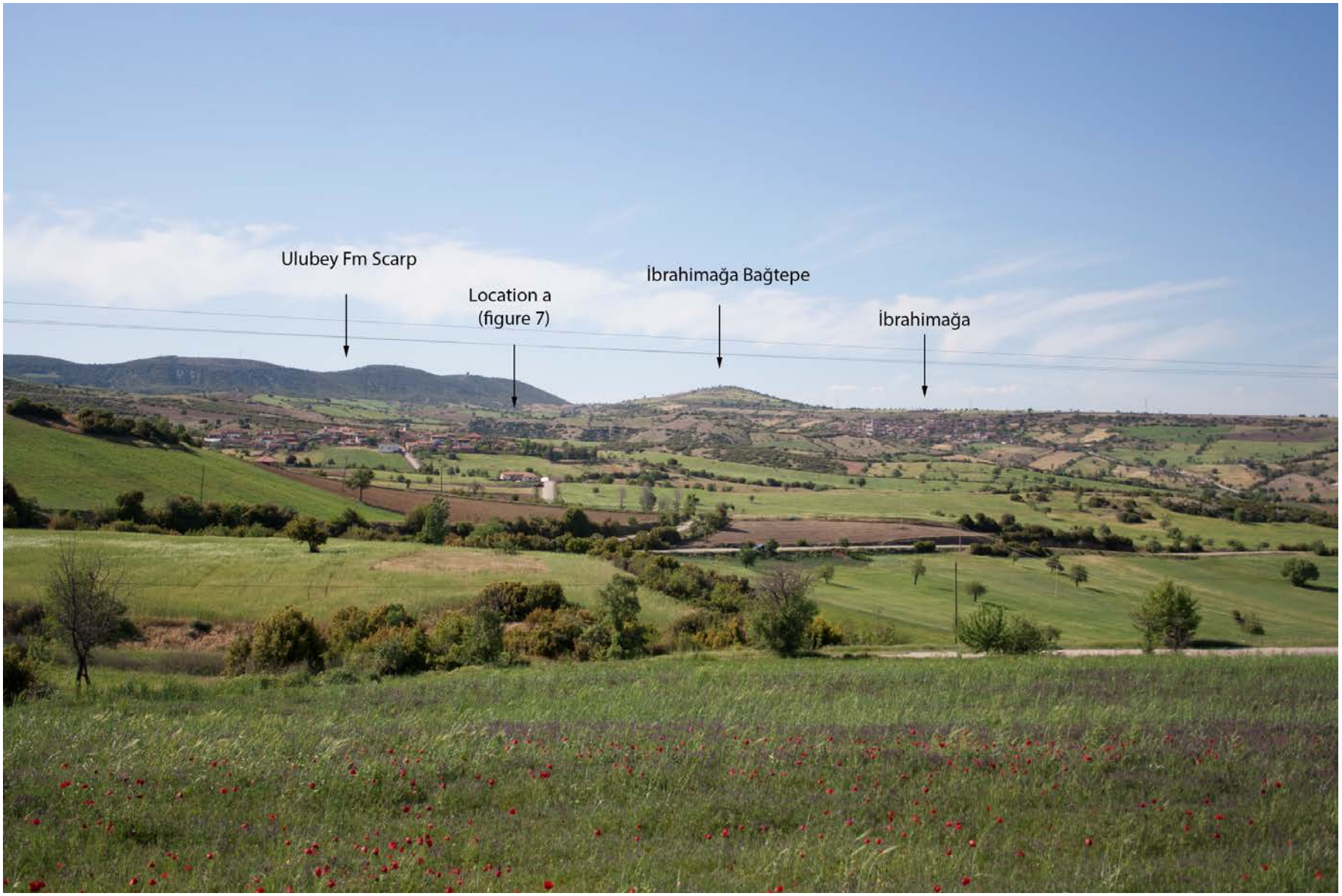
Ulubey Fm Scarp
Location a
(figure 7)
İbrahimağa Bağtepe
İbrahimağa

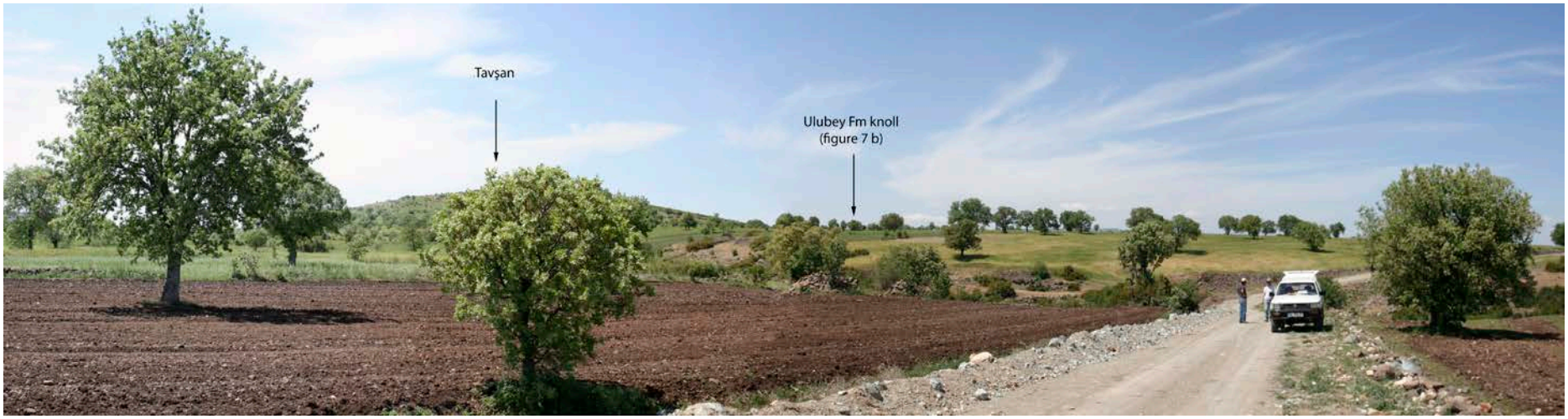
Tavşan
Ulubey Fm knoll
(figure 7 b)


Ulubey Fm. outcrop
in f3 footwall
(figure 7 c)
Location e f4
(figure 7 e)